If referring to the paper please cite the published version:

Shephard, G.E., Weirs, S., Bazhenova, E., Perez, L.F. Ramirez, L.M.M., Johansson, C., Jakobsson, M. O'Regan, M., 2018. A North Pole thermal anomaly? New heat flow measurements from the central Arctic Ocean. Journal of Geodynamics (Arctic Special Issue) https://doi.org/10.1016/j.jog.2018.01.017

A North Pole thermal anomaly? Evidence from new and existing heat flow measurements from the central Arctic Ocean

Authors: G.E. Shephard[1*], Steffen Wiers[2], Evgenia Bazhenova[3,4], Lara F. Pérez [5], Luz María Mejía[6], Carina Johansson[7], Martin Jakobsson[7], Matt O'Regan[7]

1. Centre for Earth Evolution and Dynamics (CEED), Department of Geosciences, University of Oslo, Oslo, Norway.
2. Department of Earth Sciences, Natural Resources and Sustainable Development, Uppsala University, Uppsala, Sweden.
3. Center for Coastal and Ocean Mapping, University of New Hampshire, Durham, NH, USA
4. Institute of Earth Sciences, St. Petersburg State University, St Petersburg, Russia
5. Department of Geophysics, Geological Survey of Denmark and Greenland (GEUS), Copenhagen, Denmark.
6. Geological Institute, Department of Earth Sciences, ETH, Zürich, Switzerland
7. Department of Geological Sciences, Stockholm University, Stockholm, Sweden.

* Corresponding author: g.e.shephard@geo.uio.no

Keywords: Heat flow; plate tectonics; Lomonosov Ridge; Eurasia Basin; Amundsen Basin; North Pole

Abstract:
Constraining the thermal evolution of the Arctic Ocean is hampered by notably sparse heat flow measurements and a complex tectonic history. Previous results from the Lomonosov Ridge in the vicinity of the North Pole, and the adjacent central Amundsen Basin reveal varied values, including those higher than expected considering plate cooling or simple uniform stretching models. Furthermore, in the vicinity of the North Pole an anomalously slow velocity perturbation exists in upper mantle seismic tomography models. However, whether these observations are related to a thermal anomaly in the mantle remains unknown. We present new heat flow results gathered from 17 sediment cores acquired during the "Arctic Ocean 2016" and "SWERUS-C3" expeditions on the Swedish icebreaker *Oden*. Three sites located on oceanic lithosphere in the Amundsen Basin between 7°W-71E° reveal surface thermal conductivity of 1.07-1.26 W/mK and heat flow in the order of 71-95 mW/m^2, in line-with or slightly higher (1-21 mW/m^2) than expected from oceanic heat flow curves. These

results contrast with published results from further east in the Amundsen Basin, which indicated surface heat flow values up to 2 times higher than predicted from oceanic crustal cooling models. Heat flow of 49-61 mW/m^2 was recovered from the Amerasia Basin. Sites from the submerged continental fragments of the Lomonosov Ridge and Marvin Spur recovered heat flow in the order of 53-76 and 51-69 mW/m^2 respectively. When considering the additional potential surface heat flux from radiogenic heat production in the crust, these variable measurements are broadly in line with predictions from uniform extension models for continental crust. A seismically imaged upper mantle velocity anomaly in the central Arctic Ocean may arise from a combination of compositional and thermal variations but requires additional investigation. Disentangling surface heat flow contributions from crustal, lithospheric and mantle processes, including variable along-ridge rifting rates and timing, density and phase changes, conductive and advective dynamics, and regional tectonics, requires further analysis.

1. Introduction:

As a consequence of cooling of the Earth's interior, measurements of surface heat flow reflect the thermal structure and tectonic evolution of a given region (Pollack et al., 1993; Stein and Stein, 1994). Generally, heat flow measurements across the globe are sparse. This is particularly true for the Arctic Ocean domain, where existing measurements of seafloor heat flow are largely restricted to the extensive continental shelf and mid-ocean ridge domains. Furthermore, the few heat flow measurements from near the North Pole display a large degree of variability (e.g. (O'Regan and Moran, 2010), including estimates that are higher than those predicted by thermal models for oceanic lithosphere (e.g. (Urlaub et al., 2009) and uniform crustal stretching models (O'Regan et al., 2008). The existence and/or mechanism for such a 'thermal anomaly' at the North Pole has not yet been fully explored. As part of the six-week "Arctic Ocean 2016" expedition (AO16) a number of sediment cores were acquired within the Eurasia and Amerasia basins (Figure 1). This permitted a valuable opportunity to add key localities to the global heat flow database for sites in the northern Amundsen Basin in the vicinity of the North Pole.

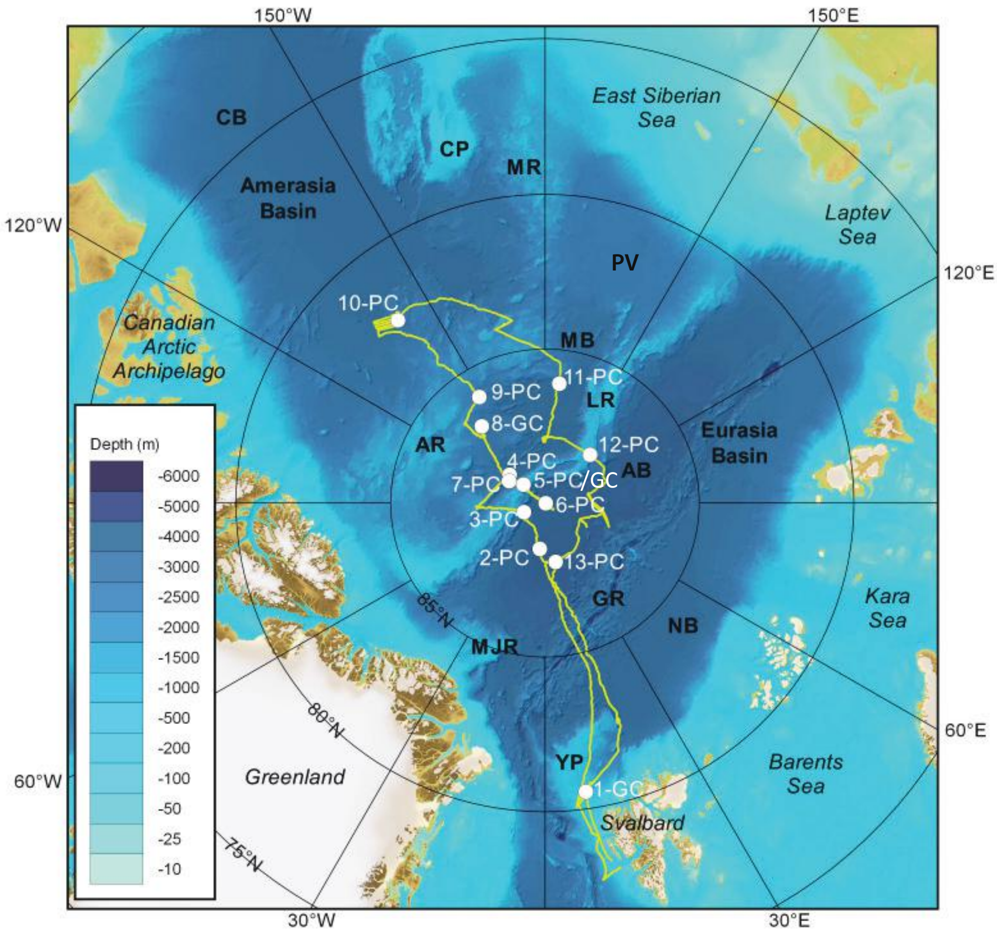

Figure 1. Overview of Arctic Ocean region, showing topography and bathymetry (IBCAO; (Jakobsson et al., 2012). Ship track from AO16 expedition in yellow and the 13 sediment coring sites in white circles with corresponding numbers for gravity core (GC) and piston core (PC). AB Amundsen Basin, AR Alpha Ridge, CB Canada Basin, CP Chukchi Plateau, GR Gakkel Ridge, LR Lomonosov Ridge, MB Makarov Basin, MJR Morris Jesup Rise, MR Mendeleev Ridge, NB Nansen Basin, PV Podvodnikov Basin, YR Yermak Plateau.

1.1 Physiography

The physiography of the Arctic Ocean is characterized by proportionally larger provinces comprised of continental shelves and ridges as compared to the rest of the world's oceans, and significant seafloor topography (Jakobsson et al., 2003; Menard and Smith, 1966). These physiographic characteristics stem from the tectonic and geodynamic history of the Arctic Ocean and the surrounding continents. The present-day thermal state of the region is therefore tied to the broadly two-phase (i.e. Mesozoic and Cenozoic) history of ocean basin opening.

The Arctic Ocean can be divided into two major ocean basins, the younger Cenozoic Eurasia Basin and older Mesozoic Amerasia Basin (Jackson and Gunnarsson, 1990) (Figure 1). These basins are distinct not only in shape, size and seafloor morphology but also in terms of their geological evolution and our overall state of knowledge concerning their formation. The older Amerasia Basin comprises the smaller Canada, Makarov and Podvodnikov basins, as well as the large Alpha-Mendeleev Ridge complex (Figure 1). The Eurasia Basin includes the abyssal plains of the Amundsen and Nansen basins, which are separated by the active mid-oceanic spreading centre - the Gakkel Ridge. The area also includes the Yermak Plateau and Morris Jesup Rise (Figure 1) closer to the margins of Svalbard and Greenland. The Eurasia and Amerasia basins are separated by the Lomonosov Ridge, an elongated, submerged continental fragment, around 1650 km in length and 50-200 km in width, extending from north of Greenland to the Siberian shelf. The crest of the Lomonosov Ridge currently lies around 1000-1500 m below sea-level (mbsl) and is largely flat-topped with Cenozoic sediment coverage in excess of 500 m thickness in places (Jokat et al., 1995).

1.2 Tectonic setting

The Eurasia Basin is a site of active seafloor spreading and delineates the current plate boundary between the North American and Eurasian plates (Figure 2). Current seafloor spreading rates along the Gakkel Ridge are “ultra-slow,” with rates decreasing from 12.7 mm/yr in the west to 6 mm/yr near its continuation into the Laptev Sea (Vogt et al., 1979). A clearly defined set of linear magnetic anomalies reveals seafloor spreading in the Eurasia Basin since the early Cenozoic (Vogt et al., 1979), at least since magnetic Chron C24 (Brozena et al., 2003) (~53 Ma using timescale of (Gee and Kent, 2007)). However, early spreading in the Eurasia Basin from around C25 (~56 Ma) has also been postulated based on magnetic, seismic and gravity data (Brozena et al., 2003; Cochran et al., 2006), and may correspond to a pronounced 10-20 km basement high adjacent to the Lomonosov Ridge (Døssing et al., 2014). The onset of seafloor spreading at this time has also been documented further south in the North Atlantic (Gaina et al., 2002).

As with most passive rifted margins of the world, locating the continent-ocean boundary (COB) and the oldest true seafloor is challenging. The transition from continental to oceanic lithosphere along the Amundsen Basin flank of the Lomonosov Ridge is thought to be relatively abrupt. There is minimal exhumed mantle or "transitional crust" along the Lomonosov margin (Cochran et al., 2006; Jokat and Micksch, 2004), which is instead described to be delineated by fault-bounded half grabens (Jokat et al., 1992). Along the margin of the Kara and Barents Shelf, the conjugate COB is relatively well defined (Cochran et al., 2006) although restorations of the Lomonosov Ridge along with the Yermak Plateau and Morris Jesup Rise present challenges (Berglar et al., 2016); (Døssing et al., 2014).

Drilling of Lomonosov Ridge crest sediments lying above the rifting unconformity during the Integrated Ocean Drilling Programs Expedition 302 (The Arctic Coring Expedition - ACEX) also point to an early post or synrift timing for opening at ~56 Ma (Backman and Moran, 2009; O'Regan et al., 2008). While slow to ultra-slow spreading rates have occurred since breakup, e.g. 17.3 mm/yr between C25o-C23y (~56-50 Ma; (Brozena et al., 2003), or less than 15 mm/yr for all times (Cochran et al., 2003), a time-dependent variation in spreading rates is noted, including an asymmetry between the Amundsen and Nansen basins of around 10-20% (Vogt et al., 1979).

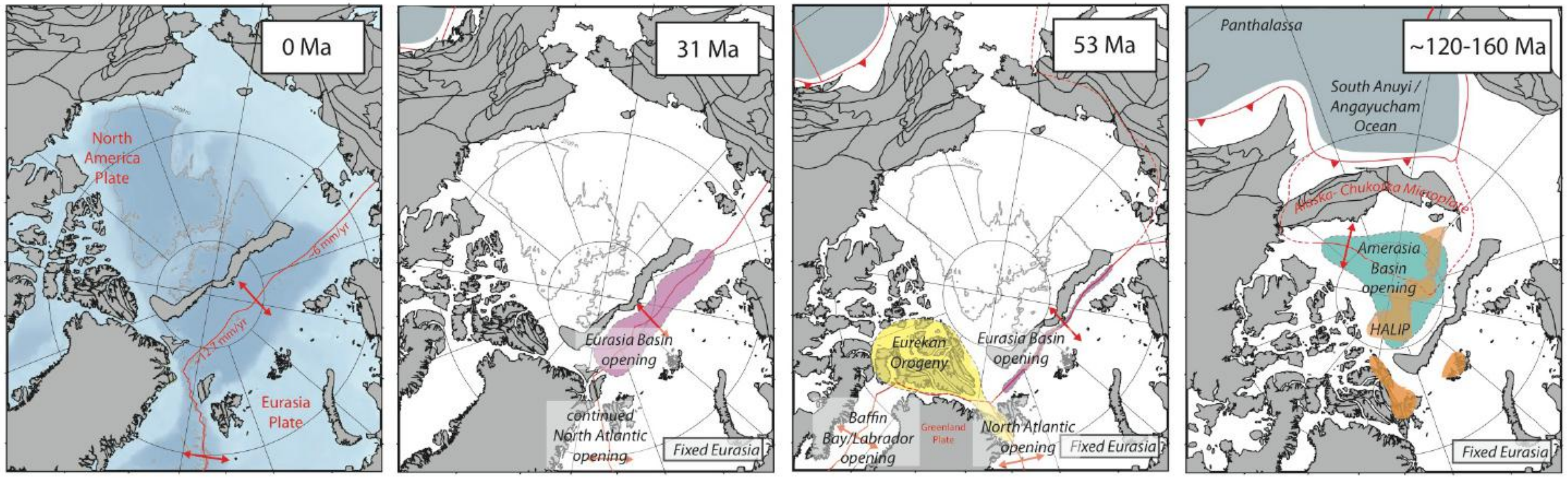

Figure 2. Tectonic reconstructions at key Mesozoic-Cenozoic Arctic events in a fixed Eurasia reference frame. Present-day for reference with bathymetry and coastlines (plus Lomonosov Ridge, Morris Jesup and Yermak Plateau) in grey, 2500 m bathymetry in the Amerasia Basin is contoured. Plate boundaries in red, modified from the plate model of (Shephard et al., 2013) and created using the *GPlates* open-source software (Williams et al., 2012). 31 Ma - opening of Eurasia Basin is continuing (purple domain), the Eurekan orogeny has just finished, and break-up of the Yermak Plateau and Morris Jesup Rise is in its final stages. The Lomonosov Ridge crest may have been at or close to sea-level at this time (O'Regan et al., 2008). 53 Ma - just after the onset of seafloor spreading in the Eurasia Basin, also during the Eurekan Orogeny (yellow domain) and opening of Baffin Bay and Labrador Sea. 160-120 Ma - broad reconstruction prior to the opening of the Amerasia Basin (green domain), showing the Alaska-Chukotka microplate restored closer to the Canadian Arctic Islands. Also displaying the approximate distribution of High Arctic Large Igneous Province (HALIP, orange polygons) that, in part, may have erupted around 121 Ma.

The Lomonosov Ridge was connected to the Barents Shelf prior to the opening of the Eurasia Basin. The earliest phases of its rifting and detachment have been the focus of recent attention including a component of initial shear/oblique motion and associated shear heating (Minakov et al., 2013), possibly starting in the Cretaceous (Berglar et al., 2016). Seafloor spreading in the region of the central part of the Lomonosov Ridge (the 'knee' like geometry) is proposed to have been delayed until around 40 Ma (Minakov and Podladchikov, 2012) or prior to C22 (~50 Ma; Cochran et al., 2006), acting as an accommodation or oblique rift zone in earlier times. In some time-dependent plate reconstructions the Lomonosov Ridge is typically fixed with respect to North America (e.g. (Gaina et al., 2002); (Rowley and Lottes, 1988; Srivastava, 1985), though unique finite rotations implying relative motion (to both Eurasia and North America) have been suggested (e.g. (Brozena et al., 2003; Jackson and Gunnarsson, 1990). A more definite interpretation and restoration is restricted due to missing or sparse magnetic, heat flow and wide-angle seismic data across the region.

A ~26 Myr sedimentary hiatus between 44.4-18.2 Ma derived from ACEX drilling results (Backman et al., 2008); (Sangiorgi et al., 2008) suggests a period of stalled post-rift subsidence until the Miocene (O'Regan et al., 2008). This delayed subsidence is at odds with the traditional post rifting subsidence models e.g. McKenzie (1978). An explanation for the delay includes far field compressional effects of the Paleocene-Eocene Eurekan Orogeny (or more broadly, a plate reorganization around C13 time), with a possible contribution of regional sea-level change (O'Regan et al., 2008). Greenland's convergence with the region of Ellesmere Island and Spitsbergen, has also been proposed to explain volcanism in the Morris Jesup and Yermak plateau prior to C13 (~34 Ma) (Brozena et al., 2003), as well as farther structural field effects within the Podvodnikov Basin (sometimes referred to more broadly as the Makarov Basin) and Laptev Sea (Gaina et al., 2015). Alternatively, a mechanism of poly-phase break up and compositional change has also been invoked to explain post-rift uplift and later rapid subsidence (Minakov and Podladchikov, 2012), at least in the central region of the Lomonosov Ridge. Thus the distribution of the associated changing stress regime related to the Eurekan Orogeny, coupled with a potential difference in crustal structure inherited from earlier rifting, as well as possible mineral phase changes, demands more attention in the context of heat flow observations.

The nature of the underlying crust in the Amerasia Basin, as well as timing and kinematics of opening and formation of these features are still widely debated. The prevailing "wind-shield wiper" model for the Amerasia Basin implies a broad counter-clockwise motion of the continental terranes of the North Slope of Alaska, Chukotka and the Chukchi Plateau, away from the Canadian Arctic Islands sometime in the Late Jurassic to Early Cretaceous (e.g. (Alvey et al., 2008; Grantz et al., 2011) (Figure 2). A related strike-slip margin has been proposed along the Lomonosov Ridge (Cochran et al., 2006), or possibly within the Alpha Mendeleev Ridge, although numerous variants and alternative regional models exist (e.g. (Miller et al., 2006); (Shephard et al., 2013).

The Alpha-Mendeleev Ridge has been variably considered as underlain by oceanic or continental basement, with a component highly intruded by magmatism related to High Arctic Large Igneous Province (HALIP) activity from around 121 Ma (e.g. (Døssing et al., 2013); (Jokat, 2003). The role of a plume in this event, and whether it was contemporaneous with opening in the Amerasia Basin is unclear. The Makarov and Podvodnikov basins, at least in part, are thought to be underlain by oceanic crust, though reported opening timings are variable, including Cretaceous or Paleogene ages (e.g. (Alvey et al., 2008); (Lebedeva-Ivanova et al., 2011).

1.3 Surface heat flow

In the absence of significant advective fluid transport, surface heat flow provides information on the conductive conditions in the underlying sediments, lithosphere and mantle. Heat flow is essentially the product of the vertical gradient of temperature and the thermal conductivity of the geological material. Typical steady state conductive heat flow measurements derived from the oceans are thought to be primarily a consequence of the age of the lithosphere, with sediment thickness providing a minor contribution (Stein and Stein, 1994). Regionally, oceanic heat flow can also be used to assess hydrocarbon potential, permafrost distribution and the presence of gas hydrates (e.g. Lachenbruch et al., 1982; (Moore and Pitman, 2011); (Lachenbruch et al., 1982; Stranne et al., 2016). Oceanic heat flow may also explain the formation of vertically homogenous deep-water bottom layers, as suggested for the Amundsen Basin near Greenland (Björk and Winsor, 2006).

Oceanic heat flow measurements are highest at mid-ocean ridges and decrease with increasing age of the lithosphere, or increasing distance from the ridge (e.g. (Von Herzen and Uyeda, 1963). On average, the heat flow from oceanic lithosphere < 10 Myrs in age is greater than ~100 mW/m^2, decaying rapidly until flattening for lithospheric ages > 50 Myrs to around 50 mW/m^2 (Parsons and Sclater, 1977). Alternative models to describe this seafloor age-heat flow (as well as depth) relationship have been proposed, including the plate models of (Parsons and Sclater, 1977) and (Stein and Stein, 1992), and half space cooling models. For our purposes, the heat flow predictions between alternative models are largely similar for seafloor ages less than ~55 Ma, although global observations for these young ages can vary significantly due to hydrothermal circulation (Lister, 1972). In addition to lithospheric age, lateral variations in oceanic heat flow may be related to horizontal variations in basement topography, sediment thickness (including radiogenic heat production and sedimentation rate), serpentinization processes, as well as shear heating, small-scale convection and mantle plumes (e.g. Hasterok et al., 2011; (Hasterok et al., 2011; Stein and Stein, 1992). Indeed, even the relationship between heat flow and sites of mantle plume-related hotspots (i.e. related to elevated sublithospheric thermal anomalies) such as Hawaii, Reunion or Iceland is not straightforward, and heat flow can be substantially scattered and/or lower than expected (e.g. Harris and McNutt, 2007; Stein and Stein, 2003).

For the GDH1 model (Stein and Stein, 1992), heat flow $\boldsymbol{q(t)}$ for oceanic lithosphere with an age ($\boldsymbol{t}$) less than 55 Ma is described by the equation:

$$q(t) = 510\ t^{(-1/2)}$$

While average global oceanic heat flow is around 101 mW/m^2, continental material is approximately 65 mW/m^2 (Pollack et al., 1993). Influences such as the last orogenic or rifting event, erosion history, as well as the radioactive content and composition of the basement will dominate the magnitude of heat flow (Sclater et al., 1980).

Although numerous models exist to predict heat flow as a function of time in extended continental crust, McKenzie's (1978) uniform extension model is the simplest and most widely applied. It is based on a set of simplifying assumptions which stipulate that i) stretching of the crust and lithosphere is uniform with depth, ii) stretching occurs instantaneously, iii) stretching is by pure shear (i.e. there is no depth dependent offset in the development of the rift zone), iv) airy isostacy is maintained throughout rift evolution, v) there is no radiogenic heat production, vi) heat flow is conductive and operates in a single dimension, and vii) the basal lithospheric temperature remains constant (Allen and Allen, 2005).

In McKenzie's model, both the surface heat flow and thermally controlled subsidence are dependent upon the amount of crustal thinning, known as the stretching factor (ß). In the uniform extension model, ß is the same for the crust and sub-crustal lithosphere. The evolution of surface heat flow through time is described by:

$$q = \frac{KT_m}{y_L}\left[1 + \frac{2\beta}{\pi}\sin\left(\frac{\pi}{\beta}\right)e^{-t/\tau}\right]$$

where q is the heat flow (mW/m^2), K is the thermal conductivity (mW/K), T_m is the basal temperature of the lithosphere, y_L is the initial lithospheric thickness, t is the time since rifting (Ma), and τ is the thermal time constant of the lithosphere defined as:

$$\tau = {y_L^2}\Big/{\pi^2 \kappa}$$

with κ being the thermal diffusivity (m/Myr).

1.4 Existing heat flow measurements

Relatively sparse measurements of marine heat flow exist in the Arctic Ocean, including both on the shelves and from the abyssal plains (Figure 3). For the older Amerasia Basin, including Alpha Ridge, heat flow measurements are limited but are generally in the order of approximately 50-60 mW/m^2 (e.g. (Taylor et al., 1986). For the Eurasia Basin, an analysis of the World Heat Flow Database (Gosnold and Panda, 2002; (Gosnold, 2002; Pollack et al., 1993) reveals a few measurements derived from the mid-oceanic Gakkel Ridge and Nansen Basin, but does not identify any existing heat flow measurements in the Amundsen Basin north of Greenland. An average heat flow of 80 mW/m^2 for the Amundsen Basin was implied based on 15 measurements collected during the RV Polarstern cruises ARK VI, ARK XVI and ARK XVII (Björk and Winsor, 2006). However, a study by (Urlaub et al., 2009) with measurements located further to the east provided heat flow estimates of 104-127 mW/m^2 for the Amundsen Basin near the North Pole (diamond symbols, Figure 3). The authors noted that given the age of the ocean crust, this was over double the magnitude predicted by the GDH1 thermal cooling model, and was not readily explainable by sediment, crustal or lithospheric scale effects.

As a fragment of rifted continental lithosphere, both submerged and with variable sedimentary cover, calculated heat flow from the Lomonosov Ridge is expected to depart from those of the Amundsen Basin. Indeed, existing measurements of heat flow from the Lomonosov Ridge show large heterogeneity (Figure 3). Those in the database include (Lubimova et al., 1973), and contain values from the Lomonosov Ridge (including some possibly near the foot) in the order of 39-89 mW/m^2. A single site from the Lomonosov Ridge with heat flow of 64-67 mW/m^2 (two values depending on methodology) was recently reported by

(Xiao et al., 2013), in the range derived from the LOREX expedition (60-65 mW/m^2, Langseth et al., 1990; (Langseth et al., 1990; Sweeney et al., 1982). (O'Regan et al., 2008) noted that surface heat flow in the range of 60-70 mW/m^2 was slightly higher (by 10-20 mW/m^2) when compared to predictions made using McKenzie's uniform extension model, assuming moderate to large stretching factors (1.1-1.8), given the time since rifting. However, no attempt was made to reconcile these observations given possible inputs from radiogenic heat production in the crust.

To date, no attempt has been made to integrate and explain observations on surface heat flow in the Amundsen Basin with those on the adjacent Lomonosov Ridge and the Amerasia Basin. Here we integrate multiple data-sets, and combine these with new measurements of surface heat flow to investigate the thermal state of the present-day North Pole region. The fundamental questions driving this effort include: are the Amundsen Basin and/or surrounding regions anomalously warm? Are the reportedly high oceanic heat flow values in the Amundsen Basin (Urlaub et al., 2009) consistent across the basin? Furthermore, is there any evidence of elevated surface heat flow values for the adjacent Lomonosov Ridge and older Amerasia Basin, and do these patterns in surface heat flow point to a broader mantle-sourced thermal and/or compositional anomaly?

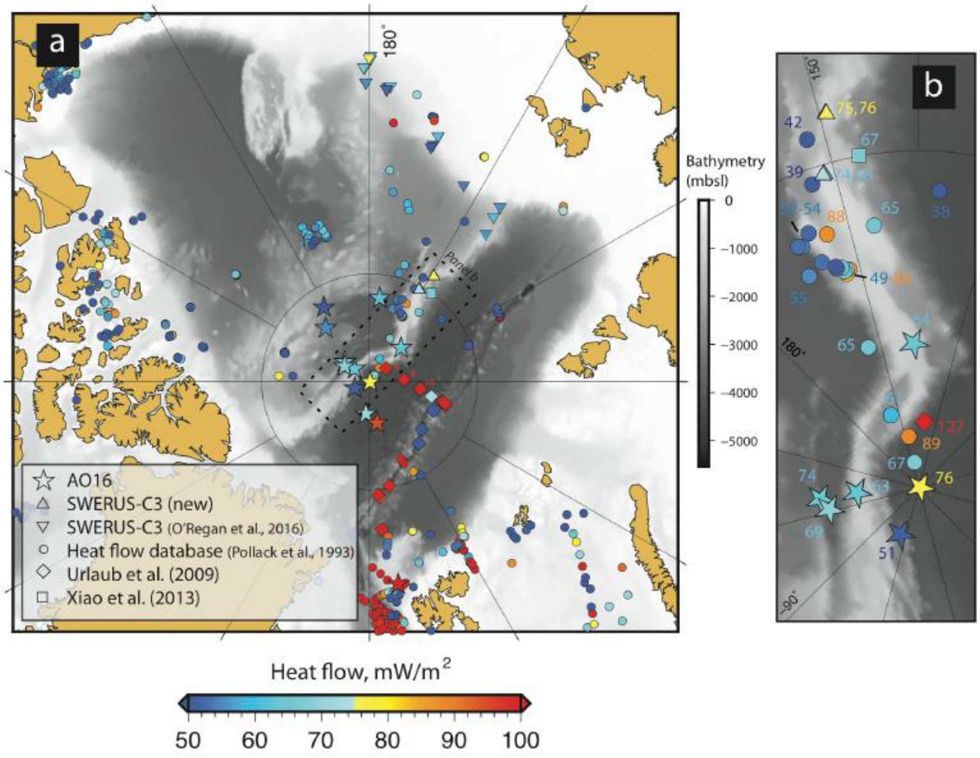

Figure 3. a. Overview of published and new Arctic heat flow studies coloured by heat flow magnitude. Inset legend for symbology; AO16 (presented here), SWERUS-C3 (O'Regan et al., 2016) and new SWERUS-C3 locations (presented here), World Heat Flow Database (sourced from [*http://www.datapages.com/gis-map-publishing-program/gis-open-files/global-framework/global-heat-flow-database, accessed May 2017*](http://www.datapages.com/gis-map-publishing-program/gis-open-files/global-framework/global-heat-flow-database)), study of (Urlaub et al., 2009) (their sites 8, 9 and 10 labelled) and a single site from (Xiao et al., 2013). b. Zoom into the central Lomonosov Ridge region with reported heat flow values shown.

2. Methods:

The majority of the new surface heat flow measurements presented here were taken during the AO16 expedition in August-September 2016, involving the icebreakers *Oden* and *Louis S. St-Laurent.* An additional new four measurements are reported from the Lomonosov Ridge (north of 84°N), and were collected during the 2014 SWERUS-C3 expedition on the Swedish icebreaker *Oden*. Other data collected on SWERUS-C3 along the East Siberian continental margin was previously published by O'Regan et al. (2016).

During AO16, sediment coring was successfully undertaken at 13 sites across the Eurasia and Amerasia basins (Table 1). A piston (with trigger weight) and/or gravity corer was used depending on bathymetric and sedimentary conditions. The recovery for the three 6 m gravity cores, two 12 m piston cores and remaining 9 m piston cores were on average 59%, 84%, and 82 %.

For context, we note that in addition to the sediment coring component, a geophysical program was included in AO16. This comprised high resolution multibeam bathymetric mapping, chirp sub-bottom profiling, water column imaging, and reflection and refraction seismics. The seismic components along with dredging were undertaken as part of Canada's extended continental shelf claim under the United Nations Convention on the Law of the Sea (UNCLOS).

Table 1. Summary of AO16 core location information and the additional sites from SWERUS-C3 expedition. PC = piston core, GC = gravity core. Trigger weight cores are not listed.

AO16-2-PC1, AO16-6-PC1 and AO16-13-PC1 were used for the in situ oceanic heat flow measurements from the Amundsen Basin discussed here. The location of all cores are shown on the map in Figure 1.

Core Label	**Location**	**Latitude (°N)**	**Longitude (°E)**	**Water depth (m)**	**Recovered length (m)**
AO16-1-GC1	Yermak Plateau	80.5532	8.0520	855	3.55
AO16-2-PC1	Amundsen Basin	88.5022	-6.6195	4353	9.45
AO16-3-PC1	Foot of Lomonosov Ridge	89.2530	-66.6097	3777	7.74
AO16-4-PC1	Marvin Spur	88.5290	-128.5048	3936	7.83
AO16-5-GC1#	Crest of Lomonosov Ridge	89.0813	-130.6800	1249	3.45
AO16-5-PC1#	Crest of Lomonosov Ridge	89.0780	-130.5470	1253	6.16
AO16-6-PC1#	North Pole (Amundsen Basin)	89.9777	71.3810	4233	7.83
AO16-7-PC1	Marvin Spur	88.6332	-121.4477	3941	8.31
AO16-8-GC1	Alpha Ridge	86.7795	-140.6433	2620	3.59
AO16-9-PC1	Alpha Ridge	85.9557	-148.3258	2212	7.52
AO16-10-PC1*	Nautilus Basin	82.3980	-141.2450	2872	7.96
AO16-11PC1	Makarov Basin	86.0993	173.1877	3066	7.98
AO16-12-PC1	Crest of Lomonosov Ridge	87.8577	136.9875	1269	5.19
AO16-13-PC1#	Amundsen Basin	88.0573	10.1850	4367	10.58
SWERUS-32-GC1	Lomonosov Ridge	85.132313	151.569013	834	2.79
SWERUS-32-GC2	Lomonosov Ridge	85.152613	151.664309	828	2.57
SWERUS-33-GC1	Lomonosov Ridge	84.274873	148.735319	886	3.63
SWERUS-33-PC1	Lomonosov Ridge	84.282038	148.646753	888	6.25

** AO16-10-PC was not included the in-situ heat flow analysis*

 # AO16-5-PC1, AO16-5-GC1, AO16-6-PC1 and AO16-13-PC1 were not split for thermal properties onboard Oden.

2.1 In-situ heat flow and geothermal gradient measurements.

All of the piston and gravity cores (with the exception of AO16-10-PC1) were rigged with miniature temperature probes of 16 cm in length by 1.5 cm diameter (ANTARES; Pfender and Villinger, 2002), in an attempt to collect in situ temperature data. These were attached to the outside of the core barrel (Figure 4). For each deployment, between 4 to 6 probes were attached along the length of the barrel, with a separation of 0.75 - 2 m between each probe. Sensor and data recovery meant that between 3-5 probes at each site were used in the final analysis (Table 2), with a single site only having 2 reliable in-situ temperature readings. The locations of the sensors were recorded before and after deployment in case of any change in position. To avoid effects from frictional heating related to core penetration, the probes were placed inside holders within steel fins located 10 cm away from the core barrel (Figure 4). Measurements were recorded with a 1s sampling interval and have a resolution of 0.001°C. Of the 13 coring sites, only one locality (AO16-10-PC1) did not retrieve in-situ temperature measurements.

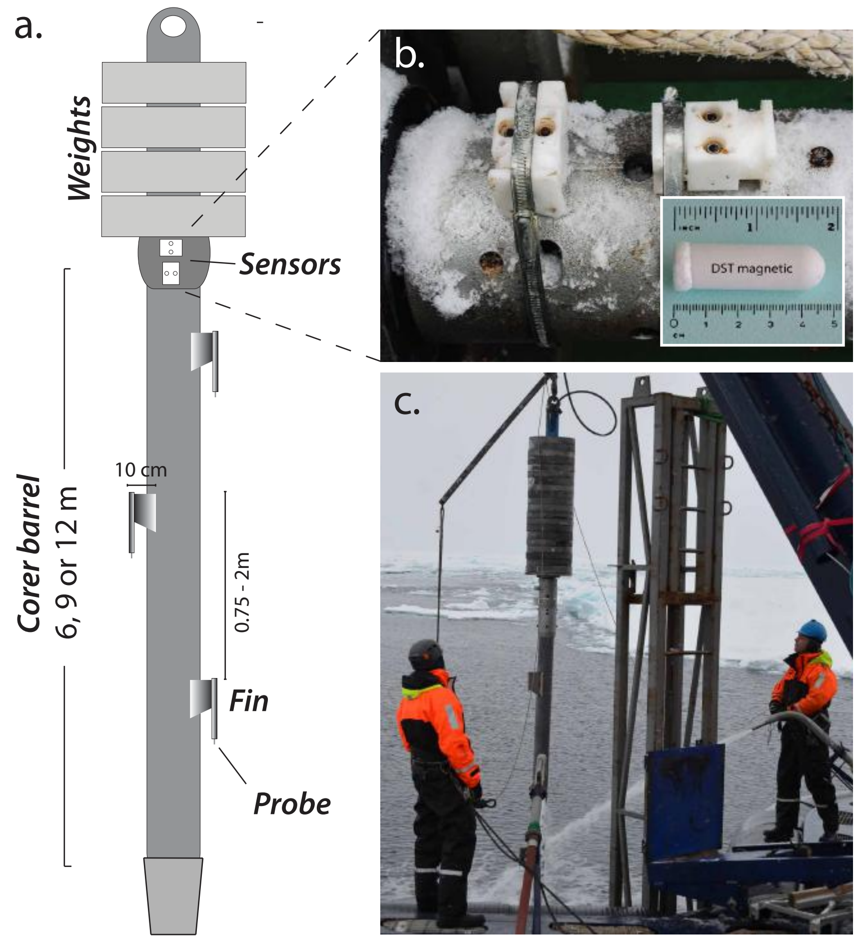

Figure 4. a. Illustration of the corer setup showing fins with temperature probes and the orientation sensors. The gravity corer was rigged for 6 m length and the piston corer for either 9 m or 12 m. ANTARES temperature probes were mounted in stainless steel fins ensuring a 10 cm distance from the core barrel (inset: close up of probe from Star Oddi, www.star-oddi.com). b. Photo of the setup of the two DST magnetic sensors, which were placed at the top of the core barrel below the weights, one in a vertical and one in a horizontal orientation (inset – actual sensor image from Star Oddi, www.star-oddi.com). c. Photo of top half of piston corer at aft deck of *Oden* during recovery.

After penetration, the corer remained within the sediment for 1.5-5 minutes (depending on water depth, drift speed and direction of the ship) to allow for thermal equilibration within the sediments. To constrain the penetration angle of the corer and/or any subsequent motions within the sediment, two orientation sensors (Star-Oddi DST magnetic) were placed near the top of the core barrel. With a 1s sampling rate, these sensors measure temperature, pressure/depth, compass heading, the xyz components of tilt, and ambient magnetic inclination and field strength. A tilt corrected temperature gradient ($\boldsymbol{T_{grad\_tilt}}$) in (°C/km) is based on the following;

$$\boldsymbol{T_{grad\_tilt}} = \frac{\boldsymbol{T_{grad}}}{\mathbf{cos}(\boldsymbol{\alpha})}$$

In which α is is the average angle of penetration and T_{grad} is the uncorrected temperature gradient (°C/km).

An “extrapolated gradient” method was used in order to calculate the geothermal gradients. Whereby a linear regression of temperature (T) versus 1/t (whereby t is time since initial sediment penetration) is used to acquire the equilibrated temperature of the sensor. When 1/t approaches 0 it is assumed that true in-situ temperature is obtained. The in-situ temperature gradient is calculated from the extrapolated temperatures for each sensor (Pfender and Villinger, 2002).

Heat flow q (Wm^{-2}) was calculated with Fourier’s Law:

$$q = \lambda \frac{dT}{dz} = \lambda\, T_{grad\_tilt}$$

In which λ is the harmonic mean of thermal conductivity, and $\frac{dT}{dz}$ is the geothermal gradient. Uncertainty estimates are also provided based on the standard error of the regression for the geothermal gradient (Table 4).

2.2 Thermal properties – conductivity, diffusivity and specific heat capacity

Sediment physical and thermal property measurements were performed on the cores typically 24-48 hours after core retrieval, and upon equilibration to room temperature (~17°C). The measurements of bulk density (from gamma ray), p-wave velocity, and magnetic susceptibility were taken in 1 cm increments on the unsplit cores using a Geotek Multi-Sensor Core Logger (MSCL).

Once split, laboratory measurements of thermal properties (thermal conductivity, diffusivity and specific heat capacity) were performed on the cores with a Hot Disk TPS 500 Thermal Constants Analyzer. 1-sided tests on 8 cores were performed onboard using a backing material of styrofoam due to its low and constrained thermal conductivity (determined during tests at beginning of cruise). A 100 g weight was placed on top of the styrofoam, and during all subsequent measurements to ensure a good contact between the sensor and the saturated sediment surface. Measurements were conducted using an 80 s heating period with a power of 0.5 watts. The intervals of thermal measurements were on average 30 cm, or upon an otherwise significant change in sediment lithology. A total of 376 measurements were performed shipboard. Due to time restrictions, cores AO16-11-PC1, AO16-6-PC1 and AO16-13-PC1 were measured onshore at Stockholm University 10 months after completion of the cruise.

We also include unpublished results from 4 sites on the Lomonosov Ridge acquired during the SWERUS-C3 cruise (Table 1 and 4). These heat flow measurements were generated with the same methodology as above, also described in (O'Regan et al., 2016).

In order to compare to the expected thermal cooling models for oceanic lithosphere, the ages of the three Amundsen Basin sites were determined from the magnetic anomaly record. Variations in past geomagnetic fields are recorded by changes in normal and reverse magnetic polarity in the seafloor, and when combined with a timescale calibrated with numerical ages (e.g. (Gee and Kent, 2007), provide key constraints on ocean basin reconstructions (Seton et al., 2012). Several catalogues of magnetic anomaly picks, and their continuations to isochrons, exist for the Amundsen and Nansen basins including those by (Brozena et al., 2003) and (Gaina et al., 2002). The three new oceanic heat flow sites in the Amundsen Basin are located on some of the oldest seafloor in the Eurasia Basin; AO16-2 near C24y (~53 Ma), AO16-6 near 25y (~56 Ma) and AO16-13 near C21y (~48 Ma).

3. Results

The in-situ temperature measurements, and derived geothermal gradients from the AO16 sites are shown in Figures 5-7, with further details and calculations of heat flow in Tables 2 and 3. The new values for the Lomonosov Ridge gathered during the *SWERUS-C3* cruise are shown in Table 4. Figure 8 shows depth versus thermal conductivity and density for each of the cores. The bulk density is controlled by the porosity, mineralogy and grain size of the sediment, which also largely determines the thermal conductivity of the sediments. Therefore, depth dependent thermal conductivity measurements closely reflect changes in bulk density, with higher density generally corresponding to higher thermal conductivity (Figure 8).

The initial temperature-time peak (Figures 5-7, left panels), related to sediment penetration in all AO16 cores is pronounced. The exception is core AO16-1-GC1, which was deployed with a lower winch speed, thus slower penetration. The core residence time in the sediment is usually in the order of 250 seconds, except for AO16-7-PC1 and AO16-11-PC1, which were just over 50 seconds due to operational and navigational limitations.

For the three sites (AO16-2-PC1, -6-PC1 and -13-PC1) clearly located on oceanic crust in the Amundsen Basin, measured heat flow is in the order of 71-95 mW/m^2. For the highest Amundsen Basin measurement (AO16-13PC1), heat flow is up to 21 mW/m^2 greater than expected based on an oceanic cooling model. Averaged thermal conductivity for these 3 sites range from 1.07-1.26 W/mK.

For the sites located on the central Lomonosov Ridge (AO16-5-PC1, -5-GC1, -12PC1) heat flow is 53-64 mW/m^2, and near the foot of the Ridge or on the Marvin Spur (AO16-3-PC1, -4-PC1 and -7-PC1) is 51-69 mW/m^2. For the (new) SWERUS-C3 sites (Table 4) heat flow was a little higher than the AO16 Ridge sites, ranging from 68-76 mW/m^2. The Amerasia Basin sites (Alpha Ridge and Makarov Basin; AO16-8PC1, -9PC1 and -11-PC1) provide heat flow values of 49-

62 mW/m², and at the Yermak Plateau the highest recorded heat flow from the expedition was recorded, 105 mW/m².

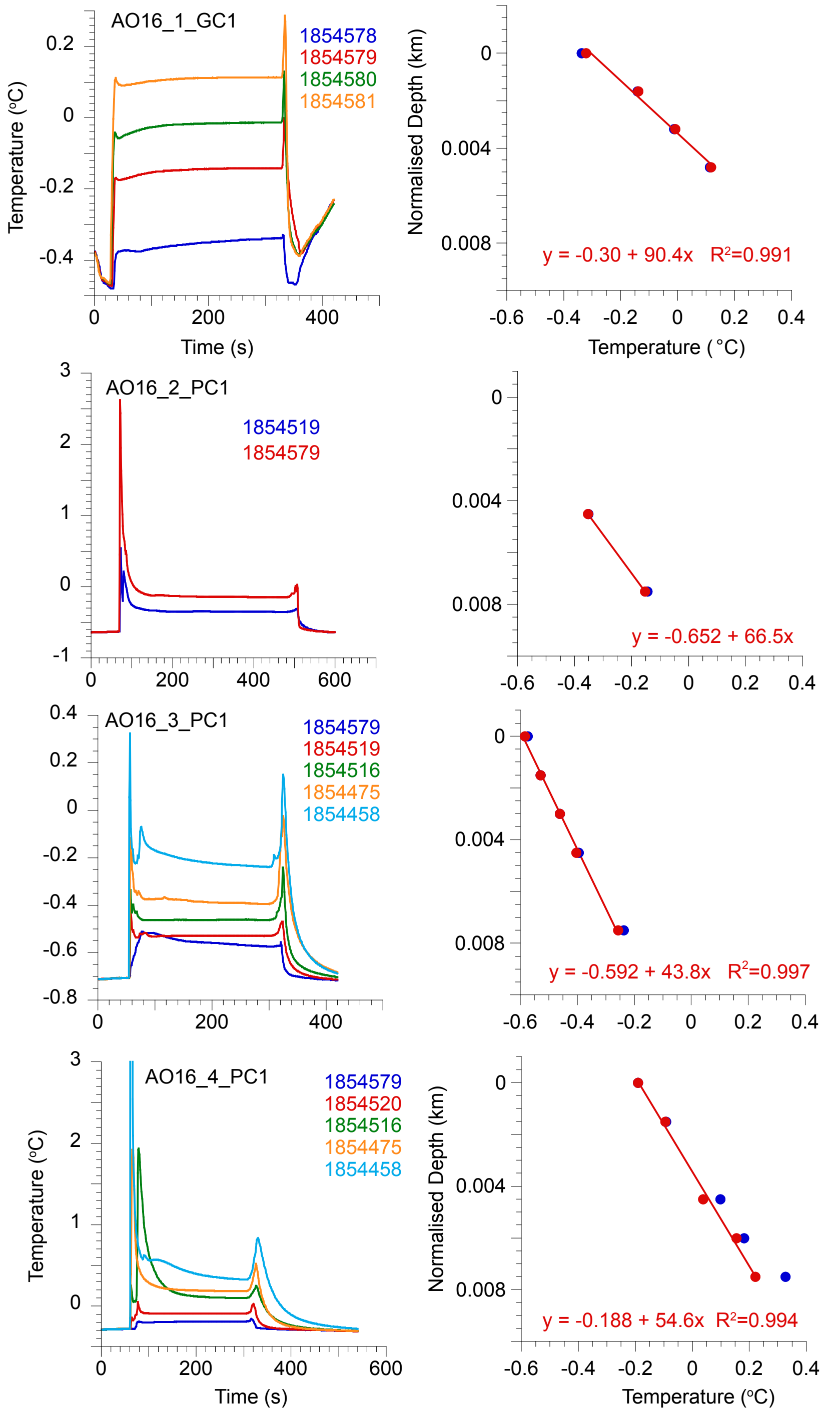

Figure 5: Temperature measurements (left panel) from individual temperature loggers at coring sites 1 to 4, and the derived geothermal gradients (right panel).

Only sensors that exhibit frictional warming upon penetration are used in the calculation of the geothermal gradients. Piston cores generally exhibit a much larger frictional heating pulse upon penetration than the gravity cores. Geothermal gradients are mostly derived from the calculated equilibrated temperature for each sensor (red) but occasionally are based on the measured temperature prior to pull out (blue) (AO16-12-PC1).

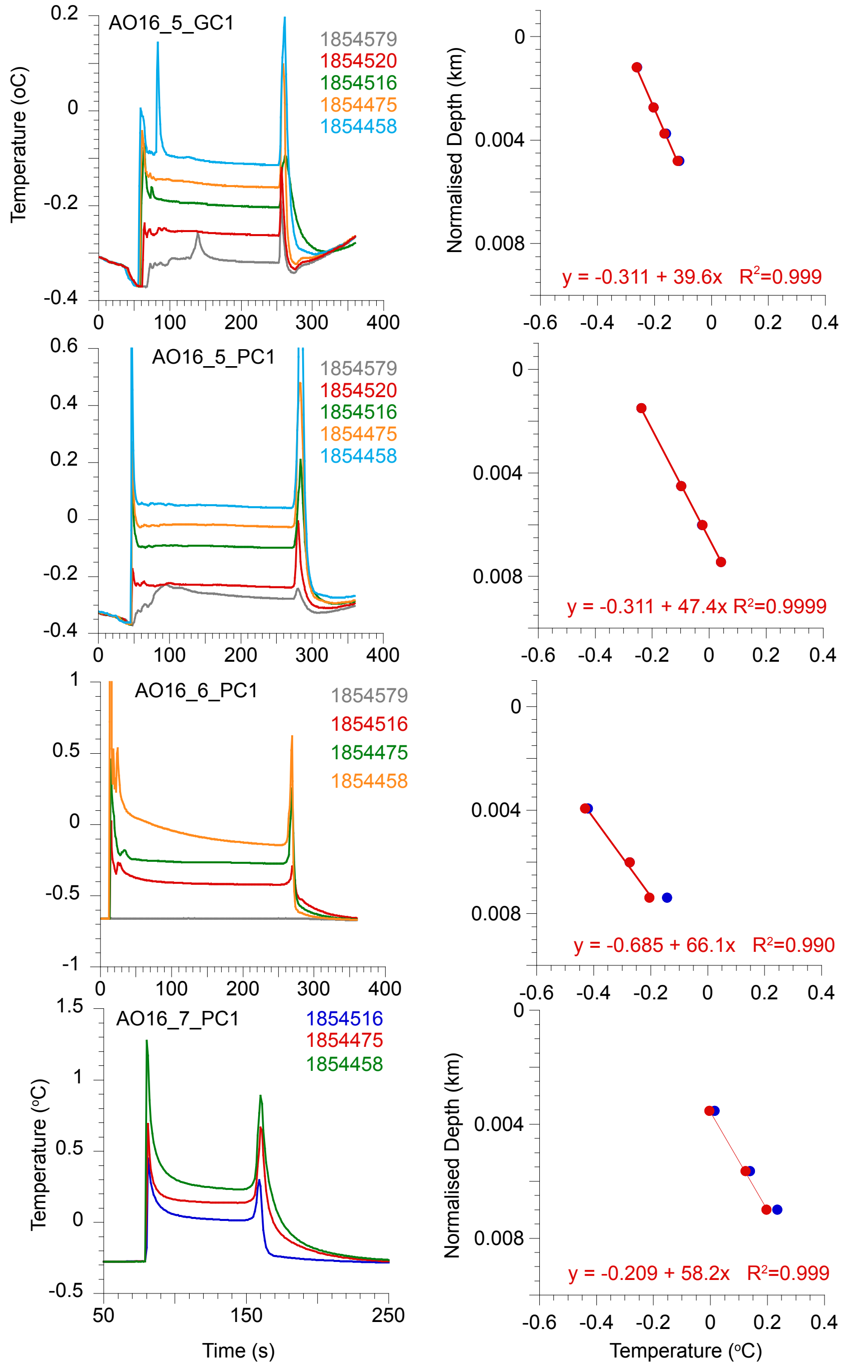

Figure 6: Temperature measurements (left panel) from individual temperature loggers at coring sites 5 to 7, and the derived geothermal gradients (right panel). Description as in Figure 5.

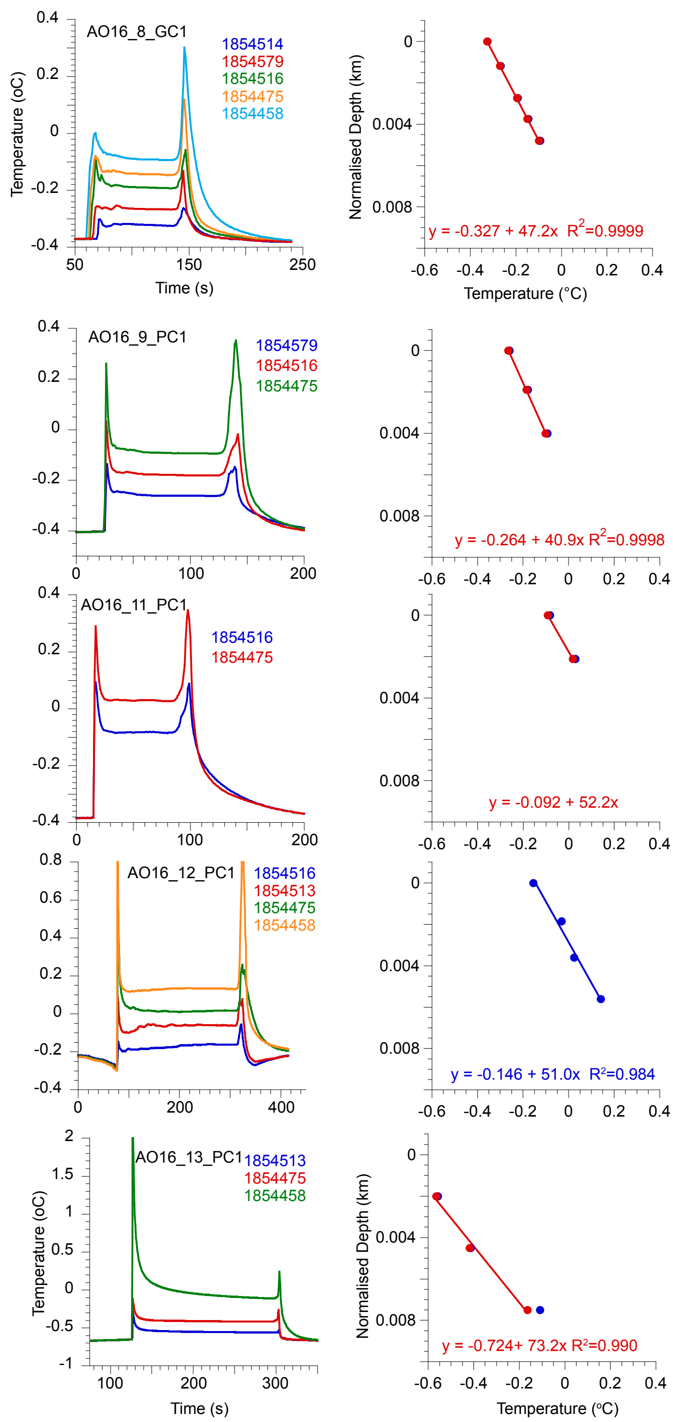

Figure 7: Temperature measurements (left panel) from individual temperature loggers at coring sites 8 to 13, and the derived geothermal gradients (right panel). Description as in Figure 5.

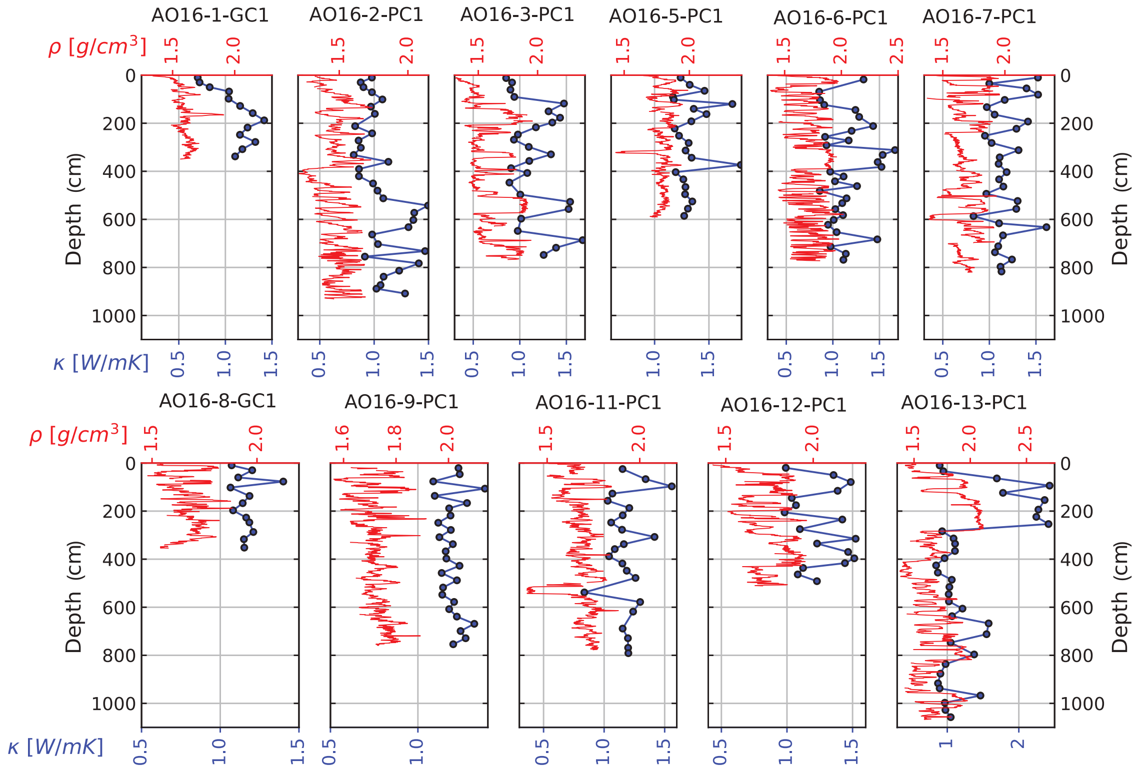

Figure 8. Thermal conductivity (kappa, blue) and density (rho, dashed red) plots for all measured AO16 cores. In case of multiple measurements at a single depth in a single core the arithmetic mean is shown instead of individual measurements. Note slightly different scales.

Table 2. Summary of thermal properties and heat flow results from AO16 sites. *Cores AO16-4PC1 and 5PC1 were not split

Core Label	Location	***Measurements from in-situ temperature probes***						***Measurements from split cores***				
		No. sensors used	***Geothermal gradient (°C/km)***	***Error (±°C/km)***	R^2	***Tilt (°)***	***Tilt corrected gradient (°C/km)***	***Average κ (W/mK)***	***St Dev. σ (W/mK)***	***No. of measurements***	***Heat flow (mW/m^2)***	***Error (mW/m^2)***
AO16-1GC1	Yermak Plateau	4	90.4	6.1	0.9909	1.0	90.4	1.17	0.16	13	105	7.1
AO16-2PC1	Amundsen Basin	2	66.5	*n/a*	*n/a*	4.2	66.7	1.07	0.20	32	71	*n/a*
AO16-3PC1	Foot of Lomonosov Ridge	5	43.8	1.3	0.9973	0.9	43.8	1.16	0.25	25	51	1.5
AO16-4PC1*	Marvin Spur	5	54.6	2.5	0.9936	0.4	54.6	*1.18*	*From 7PC1*		64	3.0
AO16-5GC1*	Crest of Lomonosov Ridge	4	39.6	1.0	0.9987	3.0	39.7	*1.33*	*From 5PC1*		53	1.4
AO16-5PC1	Crest of Lomonosov Ridge	4	47.4	0.4	0.9999	0.4	47.4	1.33	0.16	22	63	0.5
AO16-6PC1	North Pole (Amundsen Basin)	3	66.1	6.6	0.9900	4.1	66.2	1.15	0.22	31	76	7.6
AO16-7PC1	Marvin Spur	3	58.2	1.6	0.9993	0.7	58.2	1.18	0.19	29	69	1.8
AO16-8GC1	Alpha Ridge	5	47.2	0.2	0.9999	3.5	47.3	1.16	0.09	13	55	0.2
AO16-9PC1	Alpha Ridge	3	40.9	0.6	0.9998	1.7	40.9	1.20	0.07	26	49	0.7
AO16-11PC1	Makarov Basin	2	52.2	*n/a*	*n/a*	2.7	52.3	1.18	0.14	23	62	*n/a*
AO16-12PC1	Crest of Lomonosov Ridge	4	51.0	4.6	0.9989	0.6	51.0	1.26	0.20	17	64	5.8
AO16-13-PC1	Amundsen Basin	3	73.2	7.4	0.9900	4.1	73.4	1.29	0.50	34	95	9.6

Table 3. Comparison of three oceanic heat flow localities and estimates derived from half space cooling model (GDH1; (Stein and Stein, 1992))

Core Label	***Heat flow (mW/m^2)***	***Error (mW/m^2)***	***Age of lithosphere (Myr)***	***Heat flow from GDH1 (mW/m^2)***	***Difference (mW/m^2)***
AO16-2GC1	71	n/a	53	70.0	1
AO16-6PC1	76	7.6	53-56	70.0-68.2	6-7.8
AO16-13PC1	95	9.6	47	73.6	21.4

Table 4. Additional measurements from SWERUS-C3 cruise from the southern Lomonosov Ridge (Siberian margin). *Cores not split.

Core Label	***Measurements from in-situ temperature probes***									***Measurements from split cores***				
	Lat. (°N)	**Lon. (°E)**	**Water Depth (m)**	**No. Sensors used**	***Geothermal gradient (°C/km)***	***Error (±°C/km)***	***R^2***	***Tilt (°)***	***Tilt corrected gradient (°C/km)***	***Average κ (W/mK)***	***St Dev. σ (W/mK)***	***No. of measurements***	***Heat flow (mW/ m²)***	***Error (mW/ m²)***
SWERUS-32-GC1*	85.132313	151.569013	834	3	54.7	4.7	0.9930	8.5	55.3	*1.22*	*0.12*	*from 32-GC2*	68	7.1
SWERUS-32-GC2	85.152613	151.664309	828	3	59.9	3.2	0.9970	5.3	60.2	1.22	0.12	8	74	*n/a*
SWERUS-33-GC1*	84.274873	148.735319	886	4	60.7	4.1	0.9910	9.6	61.6	*1.23*	*0.08*	*from 33-PC1*	76	1.5
SWERUS-33-PC1	84.282038	148.646753	888	5	60.7	1.9	0.9970	6.5	61.1	1.23	*0.08*	18	75	3.0

4. Discussion

4.1 Is the Amundsen Basin anomalously warm?

A study by (Urlaub et al., 2009) included a 450 km long seismic transect plus heat flow measurements from the Amundsen Basin and Gakkel Ridge (Figure 3). Along their profile, one heat flow measurement was derived from near the Lomonosov Ridge (station 8, 127 mW/ m^2; at foot of slope, near possible COB), one from around 110 km further south (station 9, ~50 Ma age crust, ~2 km sediments; 104-106 mW/m^2), and another around 100 km further towards the Gakkel Ridge (Station 10, ~43 Ma, ~1.5 km sediments; 109-112 mW/m^2) (locations shown in Figures 3 and 9). While using alternative methods and setups to ours, their estimate for thermal conductivity (~1.3 W/mK) and geothermal gradients (ranging 80-98 K/km for sites 8, 9 and 10), led to significantly higher heat flow measurements than expected compared to the GDH1 model. A correlation between heat flow with basement topography or sediment thickness was not observed, serpentinization was ruled out based on gravity modelling, and Moho topography at depths of 4-7 km below the seafloor leading to elevated mantle geotherms were not favoured as an explanation. Therefore the cause of the apparent elevated heat flow in this sector of the Amundsen Basin remained unknown.

Surprisingly, results from our three stations in the Amundsen Basin do not reveal any comparably abnormal warmth. In fact they agree quite well with predictions from the GDH1 model (Table 3), arguably with the exception of site AO16-13PC1. This indicates significant variability in the thermal structure of the Amundsen Basin, and that ‘regionally’ it does not appear to be anomalously warm.

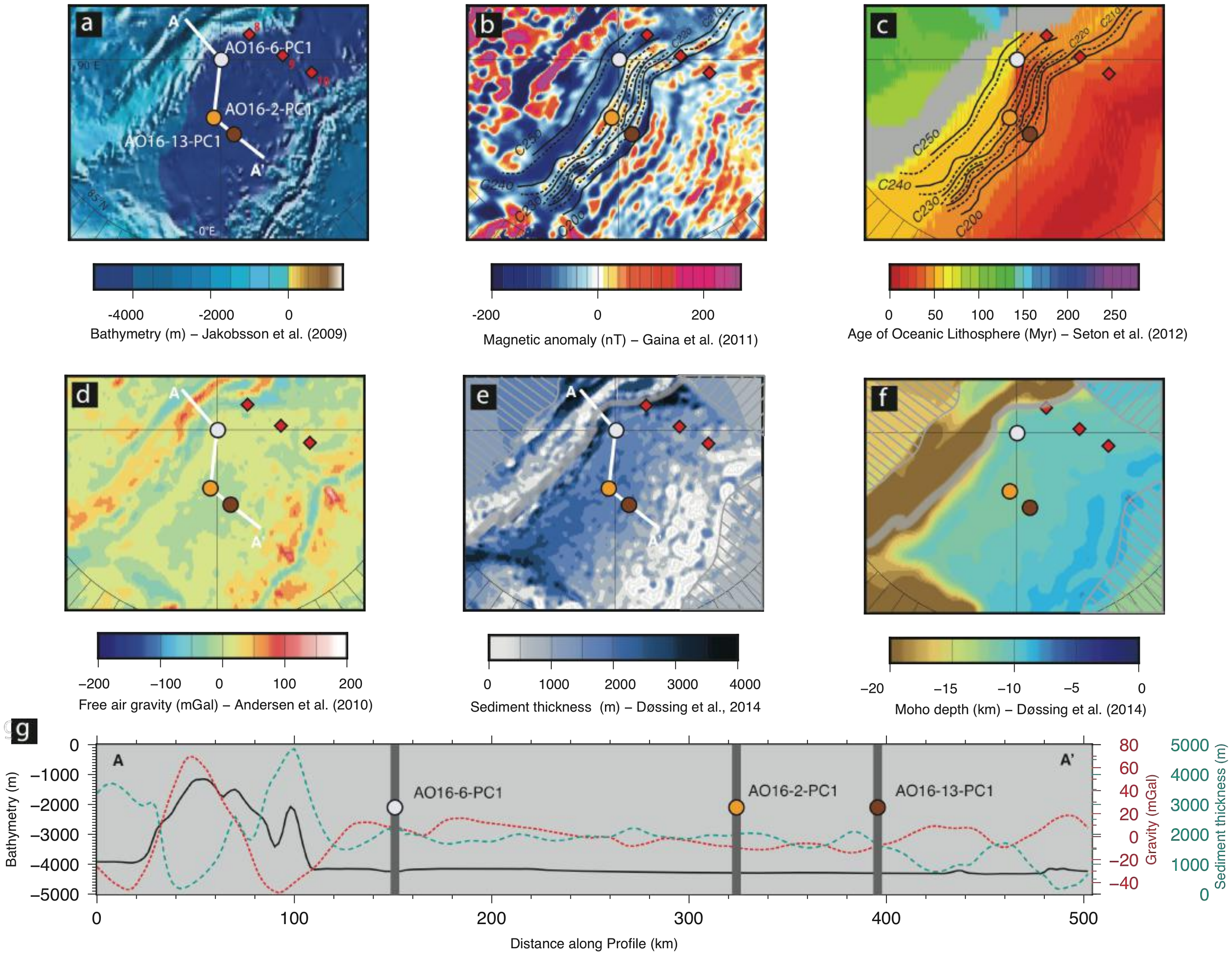

a
AO16-6-PC1
AO16-2-PC1
AO16-13-PC1
A
A'
-4000 -2000 0
Bathymetry (m) – Jakobsson et al. (2009)
b
-200 0 200
Magnetic anomaly (nT) – Gaina et al. (2011)
c
C25o
C24o
C23o
C20o
0 50 100 150 200 250
Age of Oceanic Lithosphere (Myr) – Seton et al. (2012)
d
−200 −100 0 100 200
Free air gravity (mGal) – Andersen et al. (2010)
e
0 1000 2000 3000 4000
Sediment thickness (m) – Døssing et al., 2014
f
−20 −15 −10 −5 0
Moho depth (km) – Døssing et al. (2014)
g
Bathymetry (m)
Gravity (mGal)
Sediment thickness (m)
Distance along Profile (km)
AO16-6-PC1
AO16-2-PC1
AO16-13-PC1

602

Figure 9. Overview of geophysical datasets from the western Amundsen Basin with three AO16 in-situ heat flow sites as in Figure 1 as circles, and three sites from Urlaub et al., (2009) as red diamonds. Panel a) bathymetry (Jakobsson et al., 2012), b) magnetic anomalies (Gaina et al., 2011), c) oceanic agegrid from (Seton et al., 2012) (n.b. modified to reduce gridding artifact around 90°N), solid and dashed lines show magnetic isochrons corresponding to C25 and C20 (o-old solid, and y-young dash) as derived from (Brozena et al., 2003), d) free air gravity anomaly map (Danish National Space Centre; (Andersen et al., 2010)), e) predicted sedimentary thickness (Døssing et al., 2014), f) predicted depth to Moho (from gravity modelling; (Døssing et al., 2014). Hatched areas and thick grey line in e and f were outside of the model domain/uncertain regions of (Døssing et al., 2014). Thick white line is location of transect in panel g. Panel g) Extracted profiles from panels a, d and e.

While lithospheric age is the dominant factor of oceanic heat flow, sediment cover and basement topography can also exert an influence (Stein and Stein, 1992). However, a preliminary analysis of regional geophysical datasets for sediment and crustal scale features (Figure 9) for this portion of the Amundsen Basin does not reveal any obvious differences between our stations and those from (Urlaub et al., 2009). Sedimentary cover in the central Amundsen Basin is in the order of 2-2.9 km (based on sonobuoy data from (Jokat and Micksch, 2004) and gravity modeling from (Urlaub et al., 2009). In the Amundsen Basin domain (north of Greenland), 2 km thick sediments and basement depths in excess of 6 km were modelled (Døssing et al., 2014), which shallow towards the North Pole to ~1.5 km and ~5.5 km respectively. It is worth noting that locally a broad depocenter (referred to as the North Pole Submarine Fan; (Kristoffersen et al., 2004)) with around 800 m of excess sediment coverage was predicted, and corresponds with an anomalously deep basement depth and gravity low. (Døssing et al., 2014) suggested this sub-rounded feature developed during the Eurekan compressional events related to the motion of Greenland in the Paleocene-Eocene. The Fan area includes the three AO16 Amundsen Basin sites.

The seismic reflection profiles shown in Figure 10 were acquired in the Amundsen Basin during the 2009 expedition LOMROG II. This expedition was organized as part of the Extended Continental Shelf project of the Kingdom of Denmark. The seismic equipment was formed by 1 Sercel G and 1 Sercel GI gun with a total fire pressure of 180 bar and total chamber volume of 605 cubic inches. The streamer was a 250 m long Geometrics GeoEel with 4 to 5 active sections. The shot interval was 12 s and sample rate was 1 ms. The seismic signal was processed following a standard processing sequence using ProMax software. Despite the apparent regular morphology of the seafloor, the morphology of the basement of Amundsen Basin is very irregular (Figure 10). Its depth varies between 6.5 and 8.5 s twtt (two-way travel time) below sea-level, i.e. 1 to 2.7 s twtt below seafloor. Thus, the thickness of the sedimentary cover of Amundsen Basin is very irregular, reaching ca. 2.5 s twtt in the deepest depressions of the basement (Figure 10). Such deviations in depth to basement (we cannot comment on crustal thickness) should be kept in mind in accounting for heat flow variability, but we do not think it can account for the high heat flow observations of (Urlaub et al., 2009).

While average global oceanic crustal thickness is around 6-7 km, the degree of mantle melting and crustal production, as well as ridge axis and off-axis morphology, in ultra slow end-members such as the Gakkel Ridge, is thought to be lower than for their faster counterparts (Chen, 1992). At slow spreading rates the amount of heat lost by conduction is significant and leads to a reduction in the amount of melt by mantle decompression (Bown and White, 1994). The thickness of crust formed at slow spreading centers is also more sensitive to changes in temperature (Su et al., 1994), and changes in bulk composition and rare element concentrations have also been noted for slow spreading systems (Bown and White, 1994). Observations and modelling of the youngest crust surrounding the Gakkel Ridge reveals a highly heterogenous nature and complex tectonic history (e.g. Nikishin et al., In Press; Schmidt-Aursch and Jokat, 2016). Early seismic refraction experiments in the western portion of the Amundsen Basin detail a range of crustal thicknesses, including those thinner than expected (e.g. 2-3 km; (Duckworth et al., 1982); (Jackson et al., 1982)). Based on gravity modelling, (Weigelt and Jokat, 2001) predicted 5-6 km thick crust in the Amundsen Basin. It is thus possible that variations in mantle temperatures and spreading rates along strike of the Gakkel Ridge in may explain a difference in heat flow from the western (north of Greenland) and central Amundsen Basin regions, however whether it can account for results nearly double that from GDH1 is unclear.

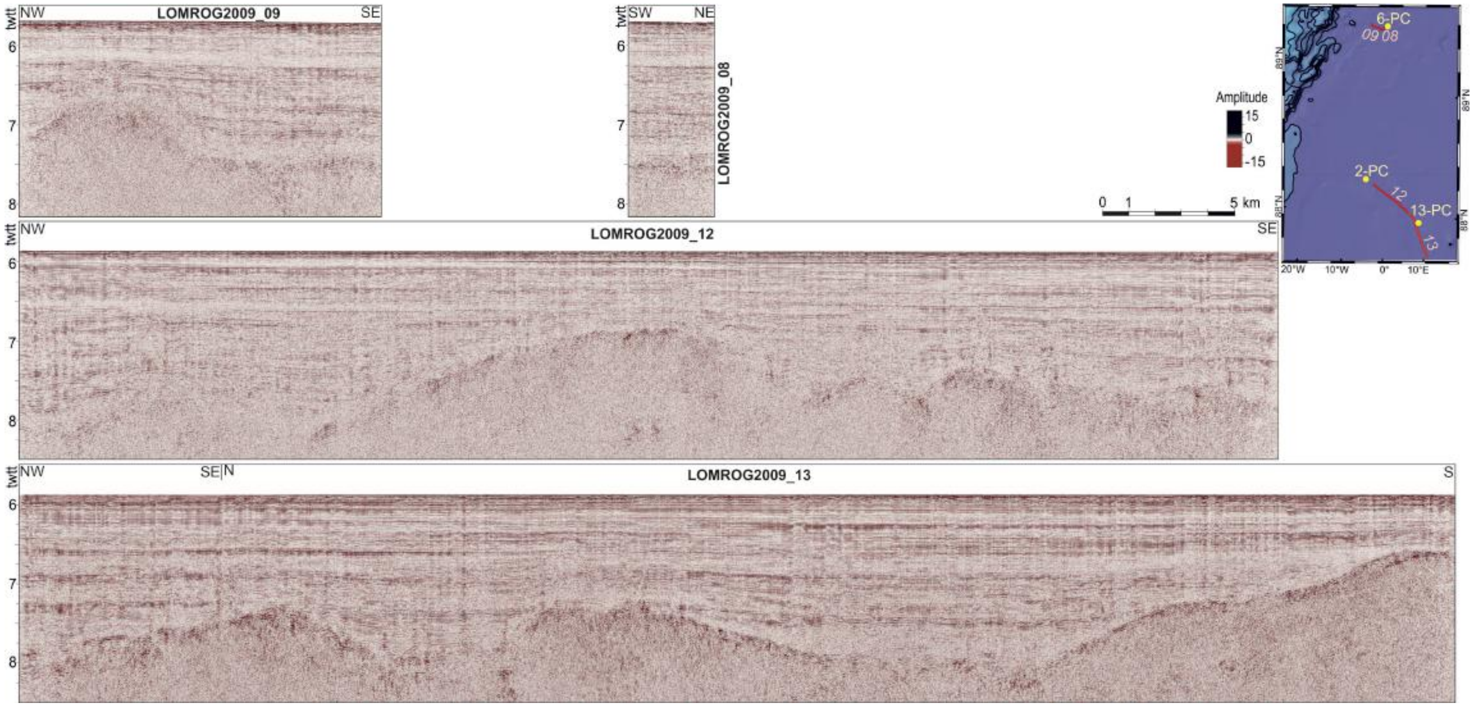

Figure 10. Seismic reflection profiles in the Amundsen Basin acquired during LOMROG II expedition under the framework of the Extended Continental Shelf project of the Kingdom of Denmark. Depth in two-way travel-time (twtt). Profiles LOMROG2009-08 & -09 are located about 1-2 km and 5 km from AO16-6PC1. Seismic line LOMROG2009-12 is located about 11 km from AO16-2PC1. Seismic profile LOMROG2009-13 is located about 800 m from AO16-13PC1. See inset map for location.

The results of our new heat flow measurements in the Amundsen Basin, 7°W-71°E north of Greenland, do not conform to those of (Urlaub et al., 2009), and instead correspond to values expected from oceanic heat flow models (largest deviation of around 20 mW/m^2). Based on our results, the Amundsen Basin sites presented here do not point to an elevated thermal anomaly. However, the *variation* in existing heat flow measurements from the Lomonosov Ridge, including those presented here, still raise an interesting point. If the high values found by (Urlaub et al., 2009) are truly representative of a local anomaly, it may thus be restricted to a domain further to the north and east (Siberian side) than our Amundsen Basin study area, and furthermore, may be relevant for discussions on the tectonic history and composition of the Lomonosov Ridge.

4.2 Thermal state of the central Lomonosov Ridge

The overall structure of the Lomonosov Ridge is variable along its length, with differences in sediment cover, depth to basement and Moho topography. Crustal thickness in the central part of the ridge is proposed to be up around 25 km (e.g. (Forsyth and Mair, 1984), with Moho depths in excess of 20-25 km closer to the Greenland margin (Jackson et al., 2010). While Bouguer gravity anomalies have been invoked to suggest relatively uniform crustal structure and thinning along the Ridge (Alvey et al., 2008; Minakov and Podladchikov, 2012), seismic imaging indicates increasing structural complexity towards the Siberian margin (south of 85°N; (Jokat, 2005). It is worth noting that crustal thicknesses along and within the Barents-Kara margin are relatively variable (Klitzke et al., 2016), and might also include the location of the Caledonide suture (e.g. (Breivik et al., 2002).

Along-strike variability in the amount and timing of rifting along the Lomonosov Ridge would lead to differences in expected heat flow based on simple uniform stretching models. This is because the upwelling of mantle and emplacement of magmatic bodies will generally lead to elevated heat flow until thermal equilibrium is reached. Pure shear and depth dependent crustal thinning also predicts significant differences in the magnitude of subsidence predicted by thermal cooling models, and thus is related to heat flow.

Based on seismic data and the current depth of the Lomonosov Ridge, (O'Regan et al., 2008) noted that heat flow measurements were higher than expected based on uniform crustal stretching models. Using a uniform stretching model with stretching factors of 1.1-1.8, the heat flow after ~56 Myrs since rifting is expected to be in the order of 42-50 mW/m^2 which is lower than measured for the Lomonosov Ridge, including for our *AO16* and (new) *SWERUS-C3* results (Table 5, Figure 11).

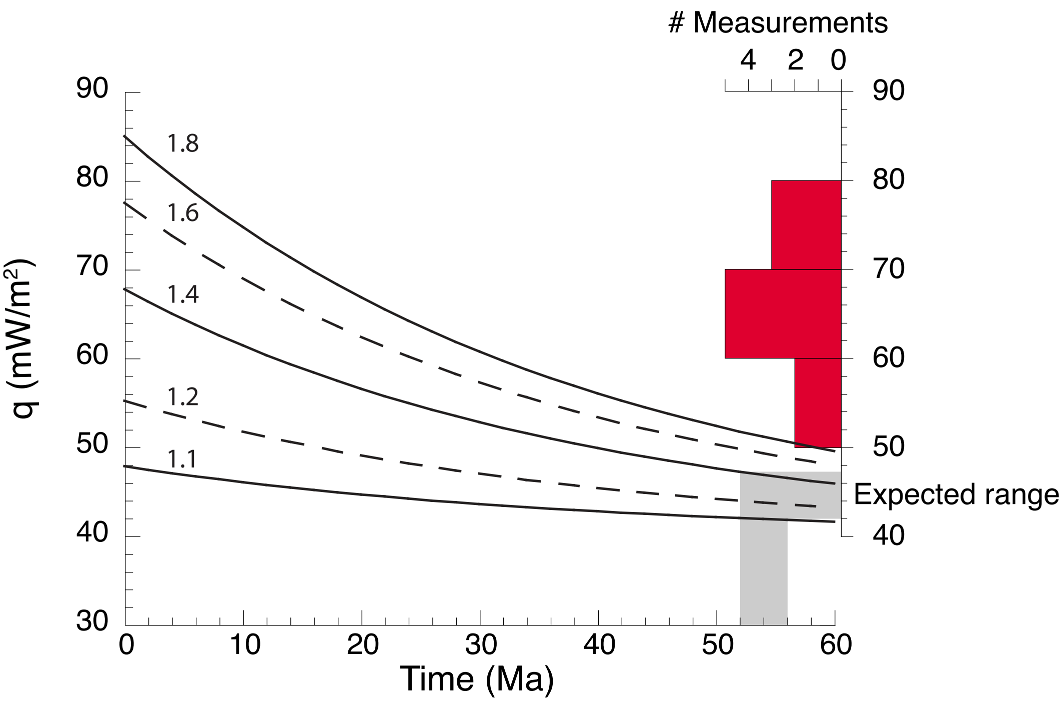

Figure 11. Heat flow predicted by (McKenzie and Bickle, 1988) uniform extension model based on a range of stretching factors (1.1-1.8) against time since rifting. Parameters listed in Table 5. The expected range for the surface heat flow on the Lomonosov Ridge is indicated for 52-56 Ma since rifting ended, and moderate stretching factors of 1.1-1.4. A histogram of new measurements from the Lomonosov Ridge and Marvin Spur (Tables 3 and 5) are shown in red. These exceed the expected range by roughly 20 mW/m. However, they have not

been corrected for radiogenic heat production in the crust, which may explain the offset.

Table 5. Parameters used to evaluate the thermal subsidence and heat flow predicted by the McKenzie (1978) uniform stretching model.

Symbol	Parameter	Units	Value
T_m	Temperature at base of lithosphere	^oC	1330
T_0	Temperature at seafloor	^oC	0
Y_L	Thickness of lithosphere	Km	110
K	Thermal conductivity of lithosphere	W/mK	3.3
κ	Thermal diffusivity of lithosphere	m^2/Ma	3.15E+07
T	Time	Ma	
τ	Thermal time constant of lithosphere	Ma	50.25
p_m	Density of mantle at 0^oC	kg/m^3	3330
α_v	Coefficient of thermal expansion for crust and mantle	$/^oC$	3.28E-05
p_w	Density of seawater	kg/m^3	1024

However, the model predictions of heat flow neglect contributions from radiogenic heat production that can account for 50–70% of the heat flux at the top of crystalline basement (Mareschal and Jaupart, 2013). The distribution of heat producing elements in the crust is highly variable, and depends on the age of formation and local composition of the crust. Generally, upper crustal rocks are the dominant contributor to radiogenic heat production. No information is available on radiogenic heat production in the continental crust of the Lomonosov Ridge. However, adopting the bulk estimate for continental crust (0.93 $\mu W/m^3$) derived from geochemical models (Rudnick and Gao, 2003), a 10-20 km thick crustal section can contribute 9.3-18.6 mW/m^3 towards the surface heat flux. This back-of-the-envelope calculation can largely reconcile the difference between the observed surface heat flow on the Lomonosov Ridge, and the coarse prediction made by McKenzie's uniform stretching model.

As such, and similar to our results from the Amundsen Basin, existing and new heat flow data from the Lomonosov Ridge does not appear to be anomalously warm. Considerable variability in the existing data can likely be explained by measurement errors and uncertainties, differences in crustal thickness and radiogenic heat production, as well as compositional differences.

4.3 Mantle structure

Beyond that of the crust and lithosphere, the deeper mantle also plays a critical role in regional thermal processes and margin evolution. Seismic velocity data provides some of the most direct constraints for the heterogenous structure of the mantle. Both temperature and composition play a key role in the density of the mantle, and are therefore intrinsic to variations of seismic velocities. However, it is generally agreed that the velocity structure in the upper mantle is dominated by temperature changes (e.g. (Forte et al., 1994) and that regions of anomalously warm mantle correspond to slow (negative) seismic wavespeed anomaly perturbations. Largely a function of source and receiver limitations, the resolution of seismic tomography under the northernmost latitudes is suboptimal. Nonetheless, the robustness of a given mantle feature can be assessed by comparing alternative tomography models, including those which have been constructed and parameterized differently.

A comparison of a recent upper mantle model SL2013sv (Schaeffer and Lebedev, 2013) with reasonable Arctic coverage, and that of a widely used whole mantle model S40RTS (Ritsema et al., 2011) reveals an overall negative seismic anomaly under the North Pole region (Figure 12) down to around 200 km depth. The conversion of seismic velocities to temperature or density anomalies is non-trivial and can be achieved through both forward and inverse methodologies, and a consideration of anelastic and anharmonic effects (e.g. (Goes et al., 2000). A full analysis incorporating sensitivities to composition, melt and temperature is beyond the scope of this study. We do not emphasize the 25 km depth slice as it is within the crustal model (CRUST2.0; (Bassin, 2000)) used in the SL2013sv tomography model.

A thermo-compositional component to explain the origins of this seismic anomaly could be considered but the degree to which the surface heat flow reflects the thermal conditions of the sublithospheric mantle in this region of the world demands further analysis. Given the variable nature of measured oceanic heat flow in reflecting elevated mantle anomalies surrounding Hawaii and Iceland (e.g. Stein and Stein, 2003), it is clear that heat flow cannot be used in isolation as a diagnostic tool for sublithospheric structure. Thus, any origins of such an uppermost mantle feature are speculative at this stage. Given the lack of a clear regional surface heat flow anomaly, i.e. existing outside the local region studied by Urlaub et al., (2009), there remains insufficient evidence to argue for a thermal anomaly underlying the central Arctic Ocean.

Any relationship between this upper mantle velocity anomaly and spreading along the Gakkel Ridge, or major regional magmatic episodes, including the High Arctic Large Igneous Province (eruption around 121 Ma, Figure 2; e.g. Corfu et al., 2013) or the North Atlantic Igneous Province (around 55 Ma; e.g. Tegner et al., 1998) – of which both eruption sites were further south from the North Pole in an absolute reference frame (Shephard et al., 2016) – are not clear. Characterizing the feature in the context of other seismically imaged features within the low-velocity zone and asthenosphere of other oceanic domains (e.g. Forsyth, 1975; Priestley and McKenzie, 2006) must also be explored. Nonetheless, we are cautious not to over interpret this anomaly, given the resolution limitation in the central Arctic Ocean.

To summarize, aside from the three Amundsen basin sites reported by (Urlaub et al., 2009), there is very little evidence for a thermal anomaly in the vicinity of the North Pole (indeed, even (Urlaub et al., 2009) did not claim there to be such). Our new data from the Amundsen basin clearly support this assertion, while the analysis of surface heat flow data on the Lomonosov Ridge does not unequivocally point towards a thermal perturbation. As discussed above, although notably higher than predictions made by the uniform extension model, the apparent discrepancy for the Lomonosov Ridge can readily be explained by moderate amounts of radiogenic heat production in the crust. Nonetheless, the potential identification of a mantle-derived feature under the North Pole requires further investigation.

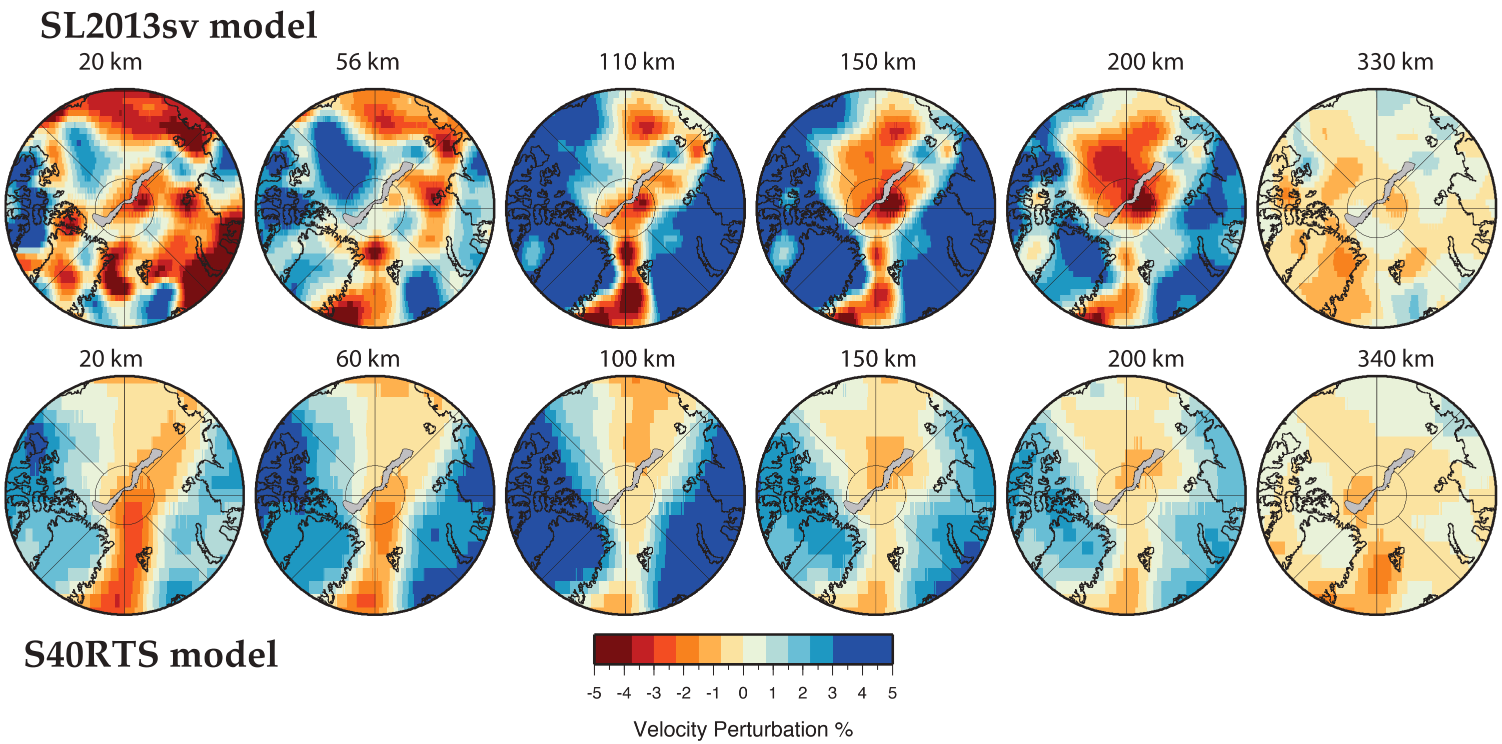

Figure 12. Depth slices through uppermost mantle from seismic tomography models of (Schaeffer and Lebedev, 2013) and (Ritsema et al., 2011). Lomonosov Ridge for reference. Red colours indicate regions of slower than average mantle (negative seismic wavespeed anomaly), possibly related to an elevated thermal and/or thermo-compositional anomaly.

Conclusions

Our new heat flow measurements for the central Arctic Ocean constitute an important constraint on the local heat flow and thermal history of this remote region. Located on oceanic lithosphere ranging from approximately 47-53 Myrs in age, heat flow in the Amundsen Basin (domain 7°W-71°E, 88-90°N) is 71-95 mW/m^2, which is broadly in line with the GDH1 plate-cooling model. This contrasts with the only other reported results from equivalently aged oceanic crust in the Amundsen Basin, which indicated a significant thermal anomaly. Furthermore, after accounting for possible radiogenic heat production, new measurements from the Lomonosov Ridge (53-69 mW/m^2) and Marvin Spur (51-69 mW/m^2), are not notably higher than predictions for moderately stretched continental crust which was last affected by major tectonic processes around 50-60 Ma. It remains unclear whether an upper mantle seismic velocity perturbation may influence regional surface heat flow, and furthermore, whether it affects regions of the Amundsen Basin outside the area where our new heat flow values exist. Our results present a generally conformable nature between model predictions and measurements of oceanic and continental heat flow in the North Pole region of the Arctic Ocean, including the Lomonosov Ridge.

Acknowledgements:

Data collection during AO16 was made possible by the captain and crew of the icebreaker *Oden,* and those onboard the icebreaker the *Louis S-St. Laurent*. The authors were supported by the Early Career Scientist Program onboard *Oden* via the Swedish Polar Research Secretariat as part of the research program SWEDARCTIC2016. The authors are grateful to the coring technicians Draupnir Einarsson and Markus Karasti. Arne Døssing is thanked for providing the relevant grids in Figure 9. We thank Peter Klitzke and Wilfried Jokat for constructive reviews.

G.E.S. is funded by VISTA – a basic research program in collaboration between The Norwegian Academy of Science and Letters, and Statoil (Project 6268, 'DEFMOD'). G.E.S. acknowledges support from the Research Council of Norway through its Centers of Excellence funding scheme, Project Number 223272. S.W. is supported by Swedish Research Council (VR) grant number 2014-4108 (Grant holder: Ian Snowball). L.F.P. acknowledges support from Geocenter Danmark. Funding for M. O. and M. J. was provided by The Swedish Research Council (VR) and the Knut and Alice Wallenberg Foundation.

Map figures created with Generic Mapping Tools (GMT) v 5.3.1 (Wessel et al., 2013) or QGIS (http://www.qgis.org/).

References

Allen, P. A., and Allen, J. R., 2005, Basin Analysis: Principles and Applications, 2nd Edition, Wiley-Blackwell.

Alvey, A., Gaina, C., Kusznir, N. J., and Torsvik, T. H., 2008, Integrated crustal thickness mapping and plate reconstructions for the high Arctic: Earth and Planetary Science Letters, v. 274, no. 3–4, p. 310-321.

Andersen, O. B., Knudsen, P., and Berry, P. A. M., 2010, The DNSC08GRA global marine gravity field from double retracked satellite altimetry: Journal of Geodesy, v. 84, no. 3, p. 191-199.

Backman, J., Jakobsson, M., Frank, M., Sangiorgi, F., Brinkhuis, H., Stickley, C., O'Regan, M., Løvlie, R., Pälike, H., Spofforth, D., Gattacecca, J., Moran, K., King, J., and Heil, C., 2008, Age model and core-seismic integration for the Cenozoic Arctic Coring Expedition sediments from the Lomonosov Ridge: Paleoceanography, v. 23, no. 1, p. n/a-n/a.

Backman, J., and Moran, K., 2009, Expanding the Cenozoic paleoceanographic record in the Central Arctic Ocean: IODP Expedition 302 Synthesis: Central European Journal of Geosciences, v. 1, no. 2, p. 157-175.

Bassin, C., Laske G., Masters, G., 2000, The current limits of resolution for surface wave tomography in North America: EOS Trans. AGU, v. 81, no. F897.

Berglar, K., Franke, D., Lutz, R., Schreckenberger, B., and Damm, V., 2016, Initial Opening of the Eurasian Basin, Arctic Ocean: Frontiers in Earth Science, v. 4, no. 91.

Björk, G., and Winsor, P., 2006, The deep waters of the Eurasian Basin, Arctic Ocean: Geothermal heat flow, mixing and renewal: Deep Sea Research Part I: Oceanographic Research Papers, v. 53, no. 7, p. 1253-1271.

Bown, J. W., and White, R. S., 1994, Variation with spreading rate of oceanic crustal thickness and geochemistry: Earth and Planetary Science Letters, v. 121, no. 3, p. 435-449.

Breivik, A. J., Mjelde, R., Grogan, P., Shimamura, H., Murai, Y., Nishimura, Y., and Kuwano, A., 2002, A possible Caledonide arm through the Barents Sea imaged by OBS data: Tectonophysics, v. 355, no. 1, p. 67-97.

Brozena, J. M., Childers, V. A., Lawver, L. A., Gahagan, L. M., Forsberg, R., Faleide, J. I., and Eldholm, O., 2003, New aerogeophysical study of the Eurasia Basin and Lomonosov Ridge: Implications for basin development: Geology, v. 31, no. 9, p. 825-828.

Chen, Y. J., 1992, Oceanic crustal thickness versus spreading rate: Geophysical Research Letters, v. 19, no. 8, p. 753-756.

Cochran, J. R., Edwards, M. H., and Coakley, B. J., 2006, Morphology and structure of the Lomonosov Ridge, Arctic Ocean: Geochemistry, Geophysics, Geosystems, v. 7, no. 5, p. n/a-n/a.

Cochran, J. R., Kurras, G. J., Edwards, M. H., and Coakley, B. J., 2003, The Gakkel Ridge: Bathymetry, gravity anomalies, and crustal accretion at extremely slow spreading rates: Journal of Geophysical Research: Solid Earth, v. 108, no. B2, p. n/a-n/a.

Døssing, A., Hansen, T. M., Olesen, A. V., Hopper, J. R., and Funck, T., 2014, Gravity inversion predicts the nature of the Amundsen Basin and its continental borderlands near Greenland: Earth and Planetary Science Letters, v. 408, p. 132-145.

Døssing, A., Jackson, H. R., Matzka, J., Einarsson, I., Rasmussen, T. M., Olesen, A. V., and Brozena, J. M., 2013, On the origin of the Amerasia Basin and the High Arctic Large Igneous Province—Results of new aeromagnetic data: Earth and Planetary Science Letters, v. 363, p. 219-230.

Duckworth, G. L., Baggeroer, A. B., and Jackson, H. R., 1982, Crustal structure measurements near FRAM II in the pole abyssal plain: Tectonophysics, v. 89, no. 1, p. 173-215.

Forsyth, D. A., and Mair, J. A., 1984, Crustal structure of the Lomonosov Ridge and the Fram and Makarov Basins near the North Pole: Journal of Geophysical Research: Solid Earth, v. 89, no. B1, p. 473-481.

Forte, A. M., Woodward, R. L., and Dziewonski, A. M., 1994, Joint inversions of seismic and geodynamic data for models of three—dimensional mantle heterogeneity: Journal of Geophysical Research: Solid Earth, v. 99, no. B11, p. 21857-21877.

Gaina, C., Nikishin, A. M., and Petrov, E. I., 2015, Ultraslow spreading, ridge relocation and compressional events in the East Arctic region: A link to the Eurekan orogeny?: arktos, v. 1, no. 1, p. 16.

Gaina, C., Roest, W. R., and Müller, R. D., 2002, Late Cretaceous–Cenozoic deformation of northeast Asia: Earth and Planetary Science Letters, v. 197, no. 3–4, p. 273-286.

Gee, J. S., and Kent, D. V., 2007, 5.12 - Source of Oceanic Magnetic Anomalies and the Geomagnetic Polarity Timescale A2 - Schubert, Gerald, Treatise on Geophysics: Amsterdam, Elsevier, p. 455-507.

Goes, S., Govers, R., and Vacher, P., 2000, Shallow mantle temperatures under Europe from P and S wave tomography: Journal of Geophysical Research: Solid Earth, v. 105, no. B5, p. 11153-11169.

Gosnold, W., Panda, B., 2002, The Global Heat Flow Database of the International Heat Flow Commission: http://www.heatflow.und.edu/index2.html.

Grantz, A., Hart, P. E., and Childers, V. A., 2011, Chapter 50 Geology and tectonic development of the Amerasia and Canada Basins, Arctic Ocean: Geological Society, London, Memoirs, v. 35, no. 1, p. 771-799.

Hasterok, D., Chapman, D. S., and Davis, E. E., 2011, Oceanic heat flow: Implications for global heat loss: Earth and Planetary Science Letters, v. 311, no. 3–4, p. 386-395.

Jackson, H. R., Dahl-Jensen, T., and the, L. w. g., 2010, Sedimentary and crustal structure from the Ellesmere Island and Greenland continental shelves onto the Lomonosov Ridge, Arctic Ocean: Geophysical Journal International, v. 182, no. 1, p. 11-35.

Jackson, H. R., and Gunnarsson, K., 1990, Reconstructions of the Arctic: Mesozoic to present: Tectonophysics, v. 172, no. 3, p. 303-322.

Jackson, H. R., Reid, I., and Falconer, R. K. H., 1982, Crustal structure near the Arctic Mid-Ocean Ridge: Journal of Geophysical Research: Solid Earth, v. 87, no. B3, p. 1773-1783.

Jakobsson, M., Grantz, A., Kristoffersen, Y., and Macnab, R., 2003, Physiographic provinces of the Arctic Ocean seafloor: GSA Bulletin, v. 115, no. 12, p. 1443-1455.

Jakobsson, M., Mayer, L., Coakley, B., Dowdeswell, J. A., Forbes, S., Fridman, B., Hodnesdal, H., Noormets, R., Pedersen, R., Rebesco, M., Schenke, H. W., Zarayskaya, Y., Accettella, D., Armstrong, A., Anderson, R. M., Bienhoff, P., Camerlenghi, A., Church, I., Edwards, M., Gardner, J. V., Hall, J. K., Hell, B., Hestvik, O., Kristoffersen, Y., Marcussen, C., Mohammad, R., Mosher, D., Nghiem, S. V., Pedrosa, M. T., Travaglini, P. G., and Weatherall, P., 2012, The International Bathymetric Chart of the Arctic Ocean (IBCAO) Version 3.0: Geophysical Research Letters, v. 39, no. 12, p. n/a-n/a.

Jokat, W., 2003, Seismic investigations along the western sector of Alpha Ridge, Central Arctic Ocean: Geophysical Journal International, v. 152, no. 1, p. 185-201.

-, 2005, The sedimentary structure of the Lomonosov Ridge between 88°N and 80°N: Geophysical Journal International, v. 163, no. 2, p. 698-726.

Jokat, W., and Micksch, U., 2004, Sedimentary structure of the Nansen and Amundsen basins, Arctic Ocean: Geophysical Research Letters, v. 31, no. 2, p. n/a-n/a.

Jokat, W., Uenzelmann-Neben, G., Kristoffersen, Y., and Rasmussen, T. M., 1992, Lomonosov Ridge—A double-sided continental margin: Geology, v. 20, no. 10, p. 887-890.

Jokat, W., Weigelt, E., Kristoffersen, Y., Rasmussen, T., and Schöone, T., 1995, New insights into the evolution of the Lomonosov Ridge and the Eurasian Basin: Geophysical Journal International, v. 122, no. 2, p. 378-392.

Klitzke, P., Sippel, J., Faleide, J. I., and Scheck-Wenderoth, M., 2016, A 3D gravity and thermal model for the Barents Sea and Kara Sea: Tectonophysics, v. 684, p. 131-147.

Kristoffersen, Y., Sorokin, M. Y., Jokat, W., and Svendsen, O., 2004, A submarine fan in the Amundsen Basin, Arctic Ocean: Marine Geology, v. 204, no. 3, p. 317-324.

Lachenbruch, A. H., Sass, J. H., Marshall, B. V., and Moses, T. H., 1982, Permafrost, heat flow, and the geothermal regime at Prudhoe Bay, Alaska: Journal of Geophysical Research: Solid Earth, v. 87, no. B11, p. 9301-9316.

Langseth, M. G., Lachenbruch, A. H., and Marshall, B. V., 1990, Geothermal observations in the Arctic region, *in* Grantz, A., Johnson, L., and Sweeney, J. F., eds., The Arctic Ocean Region, Volume L, Geological Society of America.

Lebedeva-Ivanova, N. N., Gee, D. G., and Sergeyev, M. B., 2011, Chapter 26 Crustal structure of the East Siberian continental margin, Podvodnikov and Makarov basins, based on refraction seismic data (TransArctic 1989–1991): Geological Society, London, Memoirs, v. 35, no. 1, p. 395-411.

Lister, C. R. B., 1972, On the Thermal Balance of a Mid-Ocean Ridge: Geophysical Journal of the Royal Astronomical Society, v. 26, no. 5, p. 515-535.

Lubimova, E. A., B. G. Polyak, Y. B. Smirnov, R. I. Kutas, F. V. Firsov, S. I. Sergienko, and Luisova, L. N., 1973, Heat flow on the USSR Territory: catalogue of data,: Geophys. Comm. Acad. Sci., USSR, Moscow.

Mareschal, J.-C., and Jaupart, C., 2013, Radiogenic heat production, thermal regime and evolution of continental crust: Tectonophysics, v. 609, p. 524-534.

McKenzie, D., and Bickle, M. J., 1988, The Volume and Composition of Melt Generated by Extension of the Lithosphere: Journal of Petrology, v. 29, no. 3, p. 625-679.

Menard, H. W., and Smith, S. M., 1966, Hypsometry of ocean basin provinces: Journal of Geophysical Research, v. 71, no. 18, p. 4305-4325.

Miller, E. L., Toro, J., Gehrels, G., Amato, J. M., Prokopiev, A., Tuchkova, M. I., Akinin, V. V., Dumitru, T. A., Moore, T. E., and Cecile, M. P., 2006, New insights into Arctic paleogeography and tectonics from U-Pb detrital zircon geochronology: Tectonics, v. 25, no. 3, p. n/a-n/a.

Minakov, A. N., and Podladchikov, Y. Y., 2012, Tectonic subsidence of the Lomonosov Ridge: Geology, v. 40, no. 2, p. 99-102.

Minakov, A. N., Podladchikov, Y. Y., Faleide, J. I., and Huismans, R. S., 2013, Rifting assisted by shear heating and formation of the Lomonosov Ridge: Earth and Planetary Science Letters, v. 373, p. 31-40.

Moore, T. E., and Pitman, J. K., 2011, Chapter 48 Geology and petroleum potential of the Eurasia Basin: Geological Society, London, Memoirs, v. 35, no. 1, p. 731-750.

O'Regan, M., and Moran, K., 2010, Deep water methane hydrates in the Arctic Ocean: Reassessing the significance of a shallow BSR on the Lomonosov Ridge: Journal of Geophysical Research: Solid Earth, v. 115, no. B5, p. n/a-n/a.

O'Regan, M., Moran, K., Backman, J., Jakobsson, M., Sangiorgi, F., Brinkhuis, H., Pockalny, R., Skelton, A., Stickley, C., Koç, N., Brumsack, H.-J., and Willard, D., 2008, Mid-Cenozoic tectonic and paleoenvironmental setting of the central Arctic Ocean: Paleoceanography, v. 23, no. 1, p. n/a-n/a.

O'Regan, M., Preto, P., Stranne, C., Jakobsson, M., and Koshurnikov, A., 2016, Surface heat flow measurements from the East Siberian continental slope and southern Lomonosov Ridge, Arctic Ocean: Geochemistry, Geophysics, Geosystems, v. 17, no. 5, p. 1608-1622.

Parsons, B., and Sclater, J. G., 1977, An analysis of the variation of ocean floor bathymetry and heat flow with age: Journal of Geophysical Research, v. 82, no. 5, p. 803-827.

Pfender, M., and Villinger, H., 2002, Miniaturized data loggers for deep sea sediment temperature gradient measurements: Marine Geology, v. 186, no. 3, p. 557-570.

Pollack, H. N., Hurter, S. J., and Johnson, J. R., 1993, Heat flow from the Earth's interior: Analysis of the global data set: Reviews of Geophysics, v. 31, no. 3, p. 267-280.

Ritsema, J., Deuss, A., van Heijst, H. J., and Woodhouse, J. H., 2011, S40RTS: a degree-40 shear-velocity model for the mantle from new Rayleigh wave dispersion, teleseismic traveltime and normal-mode splitting function measurements: Geophysical Journal International, v. 184, no. 3, p. 1223-1236.

Rowley, D. B., and Lottes, A. L., 1988, Plate-kinematic reconstructions of the North Atlantic and Arctic: Late Jurassic to Present: Tectonophysics, v. 155, no. 1, p. 73-120.

Rudnick, R. L., and Gao, S., 2003, 3.01 - Composition of the Continental Crust A2 - Holland, Heinrich D, *in* Turekian, K. K., ed., Treatise on Geochemistry: Oxford, Pergamon, p. 1-64.

Sangiorgi, F., Brumsack, H.-J., Willard, D. A., Schouten, S., Stickley, C. E., O'Regan, M., Reichart, G.-J., Sinninghe Damsté, J. S., and Brinkhuis, H., 2008, A 26 million year gap in the central Arctic record at the greenhouse-icehouse transition: Looking for clues: Paleoceanography, v. 23, no. 1, p. n/a-n/a.

Schaeffer, A. J., and Lebedev, S., 2013, Global shear speed structure of the upper mantle and transition zone: Geophysical Journal International, v. 194, no. 1, p. 417-449.

Sclater, J. G., Jaupart, C., and Galson, D., 1980, The heat flow through oceanic and continental crust and the heat loss of the Earth: Reviews of Geophysics, v. 18, no. 1, p. 269-311.

Seton, M., Müller, R. D., Zahirovic, S., Gaina, C., Torsvik, T. H., Shephard, G. E., Talsma, A. S., Gurnis, M., Turner, M., Maus, S., and Chandler, M., 2012, Global continental and ocean basin reconstructions since 200 Ma: Earth-Science Reviews, v. 113, no. 3-4, p. 212-270.

Shephard, G. E., Müller, R. D., and Seton, M., 2013, The tectonic evolution of the Arctic since Pangea breakup: Integrating constraints from surface geology and geophysics with mantle structure: Earth-Science Reviews, v. 124, p. 148-183.

Srivastava, S. P., 1985, Evolution of the Eurasian Basin and its implications to the motion of Greenland along Nares Strait: Tectonophysics, v. 114, no. 1, p. 29-53.

Stein, C. A., and Stein, S., 1992, A model for the global variation in oceanic depth and heat flow with lithospheric age: Nature, v. 359, no. 6391, p. 123-129.

-, 1994, Constraints on hydrothermal heat flux through the oceanic lithosphere from global heat flow: Journal of Geophysical Research: Solid Earth, v. 99, no. B2, p. 3081-3095.

Stranne, C., O'Regan, M., Dickens, G. R., Crill, P., Miller, C., Preto, P., and Jakobsson, M., 2016, Dynamic simulations of potential methane release from East Siberian continental slope sediments: Geochemistry, Geophysics, Geosystems, v. 17, no. 3, p. 872-886.

Su, W., Mutter, C. Z., Mutter, J. C., and Buck, W. R., 1994, Some theoretical predictions on the relationships among spreading rate, mantle temperature, and crustal thickness: Journal of Geophysical Research: Solid Earth, v. 99, no. B2, p. 3215-3227.

Sweeney, J. F., Weber, J. R., and Blasco, S. M., 1982, Continental ridges in the Arctic Ocean: Lorex constraints: Tectonophysics, v. 89, no. 1, p. 217-237.

Taylor, A., Judge, A., and Allen, V., 1986, Terrestrial heat flow from project CESAR, Alpha Ridge, Arctic Ocean: Journal of Geodynamics, v. 6, no. 1, p. 137-176.

Urlaub, M., Schmidt-Aursch, M. C., Jokat, W., and Kaul, N., 2009, Gravity crustal models and heat flow measurements for the Eurasia Basin, Arctic Ocean: Marine Geophysical Researches, v. 30, no. 4, p. 277-292.

Vogt, P. R., Taylor, P. T., Kovacs, L. C., and Johnson, G. L., 1979, Detailed aeromagnetic investigation of the Arctic Basin: Journal of Geophysical Research: Solid Earth, v. 84, no. B3, p. 1071-1089.

Von Herzen, R. P., and Uyeda, S., 1963, Heat flow through the eastern Pacific ocean floor: Journal of Geophysical Research, v. 68, no. 14, p. 4219-4250.

Weigelt, E., and Jokat, W., 2001, Peculiarities of roughness and thickness of oceanic crust in the Eurasian Basin, Arctic Ocean: Geophysical Journal International, v. 145, no. 2, p. 505-516.

Wessel, P., Smith, W. H. F., Scharroo, R., Luis, J., and Wobbe, F., 2013, Generic Mapping Tools: Improved Version Released: Eos, Transactions American Geophysical Union, v. 94, no. 45, p. 409-410.

Williams, S. E., Müller, R. D., Landgrebe, T. C. W., and Whittaker, J. M., 2012, An open-source software environment for visualizing and refining plate tectonic reconstructions using high-resolution geological and geophysical data sets: GSA Today, v. 22, no. 4/5, p. 4–9.

Xiao, W., Zhang, T., Zheng, Y., and Gao, J., 2013, Heat flow measurements on the Lomonosov Ridge, Arctic Ocean: Acta Oceanologica Sinica, v. 32, no. 12, p. 25-30.